nature neuroscience

Abnormal wiring of CCK$^+$ basket cells disrupts spatial information coding

Isabel del Pino[1–3,5], Jorge R Brotons-Mas[2,5], André Marques-Smith[1,4], Aline Marighetto[3], Andreas Frick[3], Oscar Marín[1,2,4,6] & Beatriz Rico[1,2,4,6]

The function of cortical GABAergic interneurons is largely determined by their integration into specific neural circuits, but the mechanisms controlling the wiring of these cells remain largely unknown. This is particularly true for a major population of basket cells that express the neuropeptide cholecystokinin (CCK). Here we found that the tyrosine kinase receptor ErbB4 was required for the normal integration into cortical circuits of basket cells expressing CCK and vesicular glutamate transporter 3 (VGlut3). The number of inhibitory synapses made by CCK$^+$VGlut3$^+$ basket cells and the inhibitory drive they exerted on pyramidal cells were reduced in conditional mice lacking ErbB4. Developmental disruption of the connectivity of these cells diminished the power of theta oscillations during exploratory behavior, disrupted spatial coding by place cells, and caused selective alterations in spatial learning and memory in adult mice. These results suggest that normal integration of CCK$^+$ basket cells in cortical networks is key to support spatial coding in the hippocampus.

The function of cortical networks relies on the precise interaction between pyramidal cells and interneurons. Interneurons are uniquely placed to orchestrate cortical activity in manifold ways due their great diversity, defined by a unique set of neurochemical, electrophysiological and morphological features[1]. Accordingly, interneurons have adopted a division of labor in cortical circuits, with distinct classes of interneurons specializing in innervating particular classes of neurons and, within them, targeting different subcellular compartments at precise time windows in reference to specific behavioral events or brain states[2,3]. Parsing the functions of different classes of interneurons is therefore crucial for unveiling how the cerebral cortex encodes information.

Basket cells comprise a heterogeneous collection of interneurons that confine their synapses to the area around the soma and primary dendrites of a target neuron, thereby exerting a powerful control over its output. There are two main classes of basket cells, with distinct developmental origins and singular neurochemical and electrophysiological properties, parvalbumin-expressing (PV$^+$), fast-spiking basket cells and cholecystokinin-expressing (CCK$^+$), regular-spiking basket cells[4–6]. CCK$^+$ basket cells are further subdivided in two main subtypes based on the mutually exclusive expression of VGlut3 or vasoactive intestinal peptide (VIP)[7].

Several lines of evidence suggest that PV$^+$ and CCK$^+$ basket cells contribute differently to cortical operations. In the hippocampus, PV$^+$ and CCK$^+$ basket cells modulate different microcircuits by preferentially targeting pyramidal cells located in deep or superficial layers of the stratum pyramidale[8]. The fast dynamics and reliable release of PV$^+$ basket cells make them suitable to operating as clocks by actively generating fast network oscillations[9,10]. In contrast, the relatively unreliable and asynchronous release of GABA by CCK$^+$ basket cells suggests a weaker contribution to gamma rhythms[11,12]. Indeed, the precise contribution of CCK$^+$ basket cells to cortical rhythms remains unknown. They may contribute to place cell firing during theta oscillations[3–5], but this hypothesis remains to be experimentally tested.

The molecular mechanisms controlling the wiring of basket cells in specific neural circuits are poorly understood[13–18]. Loss of the neuregulin receptor ErbB4 decreases the number of excitatory synapses received by PV$^+$ basket cells[14,16–18]. Here we have generated *Cck-Cre;Erbb4$^{F/F}$* mutants, containing *loxP*-flanked (*F*) alleles and expressing Cre recombinase under the control of the *Cck* promoter, to investigate the function of this receptor in the connectivity of CCK$^+$ basket cells. Because ErbB4 expression is restricted to a subset of GABAergic interneurons in the cerebral cortex[14,19], this strategy also offered a unique opportunity to investigate the consequences of disrupting the development of CCK$^+$ basket cells. In the past, the absence of unique markers for CCK$^+$ basket cells has limited the functional interrogation of this population of interneurons to single-cell analyses[12,20–22]. Our results reveal that ErbB4 is required for the normal wiring of CCK$^+$VGlut3$^+$ basket cells. These developmental defects impair the normal inhibitory function of CCK$^+$VGlut3$^+$ basket cells in the adult brain, decreases the power of theta oscillations during exploratory behavior, disrupts spatial coding by place cells, and causes selective alterations in spatial learning and memory deficits.

[1]Centre for Developmental Neurobiology, Institute of Psychiatry, Psychology and Neuroscience, King's College London, London, UK. [2]Instituto de Neurociencias, Consejo Superior de Investigaciones Científicas & Universidad Miguel Hernández, Sant Joan d'Alacant, Spain. [3]Neurocentre Magendie INSERM U1215, Bordeaux, France. [4]MRC Centre for Neurodevelopmental Disorders, King's College London, London, UK. [5]These authors contributed equally to this work. [6]These authors jointly directed this work. Correspondence should be addressed to O.M. (oscar.marin@kcl.ac.uk) or B.R. (beatriz.rico@kcl.ac.uk).

Received 6 August 2016; accepted 13 March 2017; published online 10 April 2017; doi:10.1038/nn.4544

RESULTS

Basket CCK$^+$ interneurons containing VGlut3 also express ErbB4

Nearly half of the CCK$^+$ interneurons in the mouse CA1 hippocampal area expressed VGlut3 (46%), whereas only a small fraction of them contained VIP (16%, **Fig. 1a**,**b**). Previous studies have shown that the tyrosine kinase receptor ErbB4 is abundantly expressed among CCK$^+$ interneurons[15] (**Supplementary Fig. 1a**,**b**), but it is unclear whether only a particular subset of these cells expresses ErbB4. We found that ErbB4 was prominently expressed by CCK$^+$VGlut3$^+$ interneurons (72%), but only marginally expressed by CCK$^+$VIP$^+$ ones (16%, **Fig. 1c**–**g** and data not shown). These observations therefore reveal that ErbB4 is enriched in the largest population of CCK$^+$ basket cells, which also contain VGlut3.

Wiring defects in CCK$^+$VGlut3$^+$ basket cells lacking ErbB4

Others and we have previously shown that ErbB4 plays a prominent role in the development of the connectivity of fast-spiking interneurons in the cerebral cortex[14,16,17]. To examine the function of ErbB4 in the wiring of CCK$^+$VGlut3$^+$ interneurons, we generated CCK$^+$ cell–specific conditional *Erbb4* mutants by breeding *Cck-Cre* mice[23] with mice carrying floxed *Erbb4* alleles[24]. As described before[23], *Cck-Cre* mice showed recombination in most CCK$^+$VGlut3$^+$ cells (**Supplementary Fig. 1c**,**d**). Consistently, we observed a prominent decrease in the number of CCK$^+$ and VGlut3$^+$ interneurons containing ErbB4 in the mutants compared to controls. As expected, expression of ErbB4 was maintained in interneurons lacking VGlut3 (putative PV$^+$ interneurons) (**Supplementary Fig. 2**). ErbB4 was dispensable for the generation and migration of cortical CCK$^+$ interneurons, since the density and laminar organization of CCK$^+$ cells in the hippocampus was similar between the two genotypes (**Supplementary Fig. 3**).

ErbB4 is required for the normal development of excitatory synapses onto fast-spiking interneurons[14,16,17]. In the hippocampus, ErbB4 was also prominently clustered in the somatic proximal area of CCK$^+$VGlut3$^+$ interneurons (**Fig. 1c**,**g**). We quantified the density of excitatory presynaptic inputs (VGlut1$^+$PSD95$^+$) impinging on the somata of CCK$^+$ cells at the end of synaptogenesis (postnatal day (P) 30). We found a decrease in the number of VGlut1$^+$PSD95$^+$ structures around the somata of these cells, but similar total density in *Cck-Cre;Erbb4$^{F/F}$* mutants compared to control mice (**Supplementary Fig. 4**). These results indicate that CCK$^+$VGlut3$^+$ interneurons receive a reduced number of excitatory inputs in the absence of ErbB4.

We next examined whether ErbB4 influences the establishment of the inhibitory synapses made by CCK$^+$VGlut3$^+$ interneurons. ErbB4 is present in about a quarter of the inhibitory synapses contacting the somata of pyramidal cells[14], but PV$^+$ basket cells do not require ErbB4 to make a normal complement of synapses[16,18]. One possible explanation is that ErbB4 is only present in synapses made by CCK$^+$VGlut3$^+$ interneurons. To test this hypothesis, we used antibodies for both VGlut3 and cannabinoid receptor 1 (CB1), which identifies somatic CCK$^+$ axon terminals[25], and quantified the number of VGlut3$^+$CB1$^+$ boutons contacting the somata of CA1 pyramidal cells (**Fig. 2a**,**b**). We found that the density of VGlut3$^+$CB1$^+$ boutons targeting the somata of pyramidal cells was significantly reduced in *Cck-Cre;Erbb4$^{F/F}$* mutants compared to controls (**Fig. 2c**–**e**). A similar reduction was observed in the CA3 region (data not shown). This analysis revealed that hippocampal CCK$^+$VGlut3$^+$ basket cells make fewer inhibitory synapses onto pyramidal cells in the absence of ErbB4.

Since VGlut3$^+$CB1$^+$ terminals are also very abundant around the somata of PV$^+$ interneurons in the hippocampus (**Supplementary Fig. 1e**,**f**), we hypothesized that ErbB4 might also be required for the development

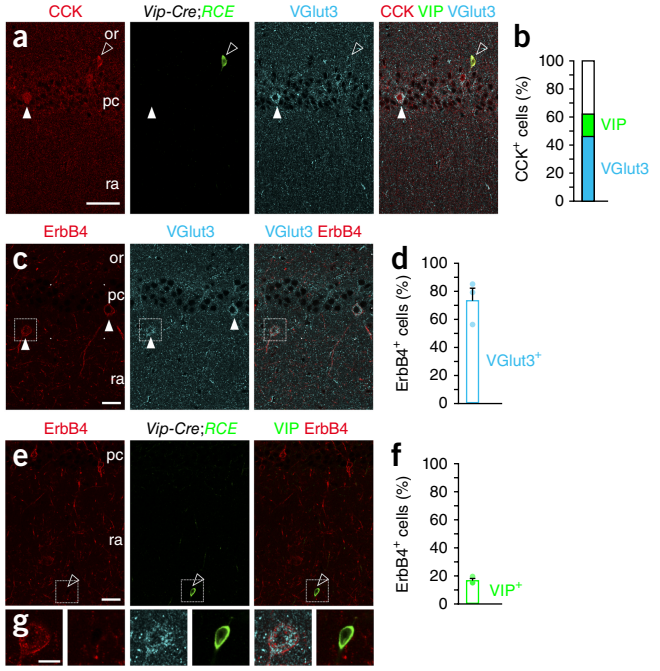

Figure 1 Subsets of CCK$^+$ interneurons express ErbB4. (**a**) Triple immunohistochemistry for CCK (red, arrowheads), GFP (green, open arrowheads) and VGlut3 (cyan, arrowheads) in the hippocampus of *Vip-Cre;RCE* mice, where *RCE* indicates *R26R* CAG-boosted *EGFP*. (**b**) Percentage of VGlut3$^+$ (cyan) and VIP$^+$ (green) cells among CCK$^+$ interneurons. (**c**) Immunohistochemistry for ErbB4 (red, arrowheads) and VGlut3 (cyan, arrowheads) in the hippocampus of *Vip-Cre;RCE* mice; $n = 166$ cells from three brains. Outlined squares in **c** and **e** are magnified in the left and right images, respectively, of each pair in **g**. (**d**) Percentage of ErbB4$^+$ cells among VGlut3$^+$ cells ($n = 112$ VGlut3 cells from three brains). (**e**) Immunolabeling showing interneurons expressing ErbB4 (red, open arrowheads) and GFP (marking *Vip* promoter activity; green, open arrowheads) in *Vip-Cre;RCE* mice. (**f**) Percentage of ErbB4$^+$ among VIP$^+$ cells ($n = 202$ VIP cells from three brains). (**g**) High magnification images from **c** (left in each pair) and **e** (right in each pair). or, stratum oriens; pc, stratum pyramidale; ra, stratum radiatum. Data are expressed as mean ± s.e.m. Scale bars, 50 µm (**a**,**c**,**e**) and 20 µm (**g**).

of these synapses. We found that PV$^+$ fast-spiking interneurons received significantly fewer VGlut3$^+$ boutons in *Cck-Cre;Erbb4$^{F/F}$* mutants than in control mice (**Fig. 2f**–**j**). In addition, we observed a decrease in total protein levels for GAD65, but not GAD67, in *Cck-Cre;Erbb4$^{F/F}$* mutants compared to control mice (**Supplementary Fig. 5**). Since GAD65 is particularly enriched in CCK$^+$ interneurons[26], these observations reinforced the notion that CCK$^+$VGlut3$^+$ basket cells have important synaptic deficits in the absence of ErbB4.

We next explored whether the synaptic deficits observed at P30 were maintained in adult mice. At P60, we found a consistent reduction in the density of CCK$^+$VGlut3$^+$ basket cell boutons impinging onto both pyramidal (**Supplementary Fig. 6a**–**d**) and PV$^+$ cells (**Supplementary Fig. 6e**–**h**) in *Cck-Cre;Erbb4$^{F/F}$* mutants. To further strengthen our conclusions, we filled VGlut3$^+$ interneurons with neurobiotin in control and *Cck-Cre;Erbb4$^{F/F}$* mutant mice and analyzed the density of varicosities per axon. We found a decrease in the density of neurobiotin-filled varicosities in *Cck-Cre;Erbb4$^{F/F}$* mutants compared to controls (**Supplementary Fig. 6i**,**j**). Taken together, our results revealed that in *Cck-Cre;Erbb4$^{F/F}$* mutants CCK$^+$VGlut3$^+$ basket cells have prominent wiring defects that begin during postnatal development and persist into adulthood.

Decreased inhibitory drive to pyramidal cells in CCK-specific *Erbb4* mutants

We investigated the functional consequences of the abnormal connectivity of CCK$^+$VGlut3$^+$ basket cells lacking ErbB4. To this end, we first recorded spontaneous inhibitory postsynaptic currents (sIPSCs) from individual CA1 pyramidal cells in acute slices from P60–70 control and *Cck-Cre;Erbb4$^{F/F}$* mutant mice (**Fig. 3a**). Pyramidal cells of *Cck-Cre;Erbb4$^{F/F}$* mutant mice exhibited a modest but significant decrease in sIPSC amplitude, with no significant changes in sIPSC frequency (**Fig. 3a–d**). Moreover, we observed no apparent changes in the intrinsic properties of CCK$^+$ interneurons (**Supplementary Fig. 7a**). These findings indicated that basal inhibitory synaptic transmission is compromised in *Cck-Cre;Erbb4$^{F/F}$* mutants.

We reasoned that compensatory mechanisms and/or polysynaptic effects could mask a more vigorous synaptic transmission phenotype. To circumvent this problem, we directly assessed the function of CCK$^+$ interneurons in *Cck-Cre;Erbb4$^{F/F}$* mutants using optogenetics. We injected the CA1 region of control and conditional mutants with adeno-associated viruses (AAV) carrying a conditional construct expressing Channelrhodopsin-2 (ChR2) fused to EYFP (**Supplementary Fig. 8a–d**). Since the *Cck* promoter drives the expression of *Cre* in pyramidal cells as well as CCK$^+$ interneurons[23], AAV injections led to ChR2 expression in both cell types, which precluded the exclusive activation of CCK$^+$ interneurons. To overcome this limitation, we developed a strategy through which we could specifically examine the inhibition arising from infected CCK$^+$ interneurons. First we recorded from control and mutant ChR2$^+$ pyramidal cells in voltage-clamp mode under GABAergic and glutamatergic blockade, obtaining *I-V* curves in response to 473-nm photostimulation (**Fig. 3e,h** and **Supplementary Fig. 8e–g**). At a holding potential of +10 mV, direct ChR2 photocurrents were negative and modest for all pyramidal cells recorded (**Supplementary Fig. 8e**, n = 21 cells, −59.1 ± 10.2 pA), which enabled us to unequivocally distinguish them from CCK$^+$ interneuron light-evoked positive synaptic GABAergic currents (**Supplementary Fig. 8f**). This observation held when splitting results by genotype (n = 15 control cells, 6 mutant cells), as there were no significant differences in photocurrent amplitude at +10 mV (Mann-Whitney U = 32, P = 0.3403, control median = −45 pA, *Cck-Cre;Erbb4$^{F/F}$* median = −60 pA). All subsequent optogenetic experiments were thus performed under glutamatergic receptor blockade, at a holding potential of +10 mV.

We then characterized light-evoked spiking in CCK$^+$ interneurons to verify that photostimulation produced similar responses in the two genotypes. Recordings were targeted to CCK$^+$ cells in CA1 stratum radiatum, where the VGlut3$^+$ population is enriched (**Supplementary Fig. 3f–h**), and revealed no effect of genotype on the number of spikes fired per stimulus (**Fig. 3e–g**). We then recorded optogenetically evoked IPSCs in CA1 pyramidal neurons (**Fig. 3h**). The peak amplitude of evoked IPSCs was significantly reduced in *Cck-Cre;Erbb4$^{F/F}$* mutants compared to controls, with multiple-comparisons testing revealing statistically significant effects for photostimulation irradiances above and including 2 mW/mm^2 (**Fig. 3i**). Gabazine completely abolished synaptic currents, confirming them to be GABAergic (**Supplementary Fig. 8g**). These results confirmed that the inhibitory input of CCK$^+$ interneurons onto pyramidal cells is functionally impaired in *Cck-Cre;Erbb4$^{F/F}$* mutants. Under optogenetic stimulation at low illumination intensities, a mixture of successes and failures in spiking could be observed (**Fig. 3g**, 0.23 mW/mm^2 irradiance), as with minimal stimulation using electrodes. For a subset of pyramidal neurons, we were able to lower illumination intensity to a point where we correspondingly observed a mixture of successes and failures in IPSCs in an all-or-none pattern (**Supplementary Fig. 8h–j**). Successfully evoked synaptic currents under these conditions are interpreted as arising from a single action potential from one

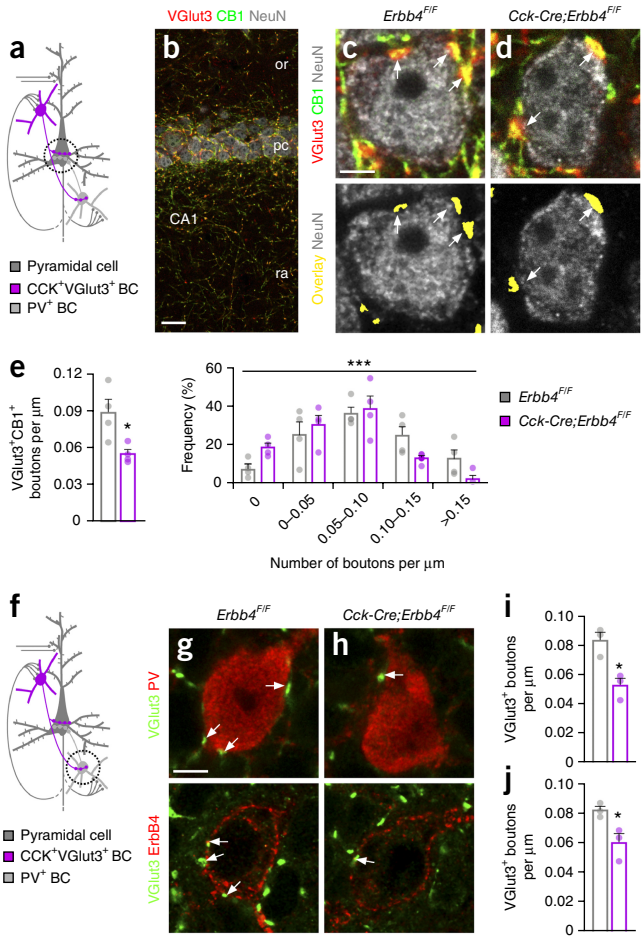

Figure 2 Deletion of *Erbb4* from CCK$^+$ interneurons decreases the number of synapses made on hippocampal pyramidal and parvalbumin cells at P30 in CA1 hippocampal region. (**a**) Schematic showing *Erbb4* deletion from CCK$^+$ interneurons. The circle indicates the synapses analyzed in this experiment. BC, basket cell. (**b**) Triple immunohistochemistry showing VGlut3 (red), CB1 (green) and NeuN staining (gray). (**c**,**d**) Top, confocal images showing high magnification of double-positive VGlut3$^+$CB1$^+$ boutons apposed to NeuN$^+$ somata in the pyramidal cell layer (arrows). Bottom, binary images used for quantification; co-localization of VGlut3 and CB1 in yellow (arrows). (**e**) Left, density of VGlut3$^+$CB1$^+$ boutons contacting the somata of pyramidal cells in control and mutant mice. t test, $t_{(6)} = 2.931$ $^*P = 0.026$, n = 366 and 280 neurons in CA1 from four controls and four mutants, respectively. Right, distribution of densities of VGlut3$^+$CB1$^+$ boutons on the somata of pyramidal cells in control and mutant mice at P30. $\chi^2 = 36.172$, d.f. = 4, $^{***}P < 0.001$, n = 366 and 280 neurons from 4 controls and 4 mutants, respectively. (**f**) Scheme of *Erbb4* deletion from CCK$^+$ interneurons. The circle indicates the synapses analyzed in this experiment. (**g**,**h**) Top, representative confocal images showing VGlut3$^+$ boutons (green, arrows) contacting a PV$^+$ interneuron (red) in control (**g**) and mutant (**h**) mice. Bottom, confocal images showing VGlut3$^+$ boutons (green, arrows) contacting an ErbB4$^+$ interneuron (red) in control (**g**) and mutant (**h**) mice. (**i**) Density of VGlut3$^+$ boutons contacting the somata of PV$^+$ interneurons. t test, $t_{(4)} = 4.048$, $^*P = 0.016$, n = 35 and 29 neurons from 3 controls and 3 mutants, respectively. (**j**) Density of VGlut3$^+$ boutons contacting the somata of ErbB4$^+$ interneurons. $^*P = 0.033$, t test, $t_{(4)} = 3.211$, n = 67 and 57 neurons from 3 controls and 3 mutants, respectively. or, stratum oriens; pc, stratum pyramidale; ra, stratum radiatum. Scale bars, 20 µm (**b**) and 3 µm (**c** and **d**, **g** and **h**). Data are expressed as mean ± s.e.m.

presynaptic neuron[27]. In the subset of pyramidal cells where minimal-intensity IPSCs could be distinguished from the direct ChR2 photocurrent, we observed that the average peak amplitude of IPSCs was significantly lower in *Cck-Cre;Erbb4*$^{F/F}$ mutants than in controls (**Fig. 3j**). The frequency distribution of all such events also suggested a shift toward lower IPSC amplitudes in the mutants (**Supplementary Fig. 8h–j**). Taken together, these results demonstrate that the inhibition of pyramidal cells by CCK$^+$ interneurons is functionally impaired in *Cck-Cre;Erbb4*$^{F/F}$ mutants.

To assess the impact of these defects on the activity of pyramidal cells, we next recorded spontaneous excitatory postsynaptic currents (sEPSCs) in CA1 pyramidal cells from acute slices at P60–70. The activity of pyramidal cells was moderately disrupted in *Cck-Cre;Erbb4*$^{F/F}$ mutants (**Supplementary Fig. 7**). Together our findings demonstrate that synaptic deficits in the wiring of CCK$^+$VGlut3$^+$ interneurons caused by the loss of ErbB4 impair the inhibition of pyramidal cells.

Reduced hippocampal theta activity in CCK-specific *Erbb4* mutants

We next sought to investigate the impact of the observed deficits *in vivo* by recording hippocampal local field potential (LFP) in freely moving control and *Cck-Cre;Erbb4*$^{F/F}$ mutant mice. We implanted tetrodes in the dorsal hippocampus and recorded LFP during spontaneous exploration in a square open field arena. *Cck-Cre;Erbb4*$^{F/F}$ mutants had a significant decrease in the power of delta and theta oscillations, with no significant changes in the theta/delta ratio, theta frequency or power of high-frequency oscillations (**Fig. 4a–h**). Since *Cck-Cre* mice do not experience recombination in the septum or brainstem pontine nuclei (**Supplementary Fig. 9**), two structures that influence theta activity in the hippocampus[28,29], the prominent decrease in the power of theta frequency observed in *Cck-Cre;Erbb4*$^{F/F}$ mutants is likely caused by defects in cortical CCK$^+$ interneurons. These observations reveal that developmental disruption of the wiring of CCK$^+$VGlut3$^+$ basket cells alters hippocampal rhythms, most notably in the theta frequency.

Spatial memory formation is altered in CCK-specific *Erbb4* mutants

We next performed a battery of behavioral tests to evaluate locomotor activity, anxiety responses and cognitive function in *Cck-Cre;Erbb4*$^{F/F}$ mutants. We found no differences in locomotion or anxiety responses between the two genotypes (**Supplementary Fig. 10a–d**). We also analyzed LFP in relation to several variables of motor behavior in control and *Cck-Cre;Erbb4*$^{F/F}$ mutant mice, finding no significant differences between genotypes (speed versus theta power $P = 0.081$; position versus theta power $P = 0.298$). These results suggested that the theta power deficits observed in the mutants are independent of the locomotor activity of the mice (**Supplementary Fig. 10e–j**).

We next used prepulse inhibition of the startle response test to analyze the ability of *Cck-Cre;Erbb4*$^{F/F}$ mutant mice to filter out unnecessary information. While the amplitude of the startle response was similar between the two genotypes, *Cck-Cre;Erbb4*$^{F/F}$ mutants failed to inhibit their startle response when the pulse was preceded by a weaker stimulus (**Supplementary Fig. 11a**). These results suggested that mutant mice have deficits in sensorimotor gating or attention.

To begin examining cognitive capabilities in *Cck-Cre;Erbb4*$^{F/F}$ mutants, we used the one-trial novel object recognition and object location tasks. These tests explore hippocampal function and are based on the natural preference of mice for novelty (**Fig. 5a,b**). Total exploration times during the test phase and discrimination indices

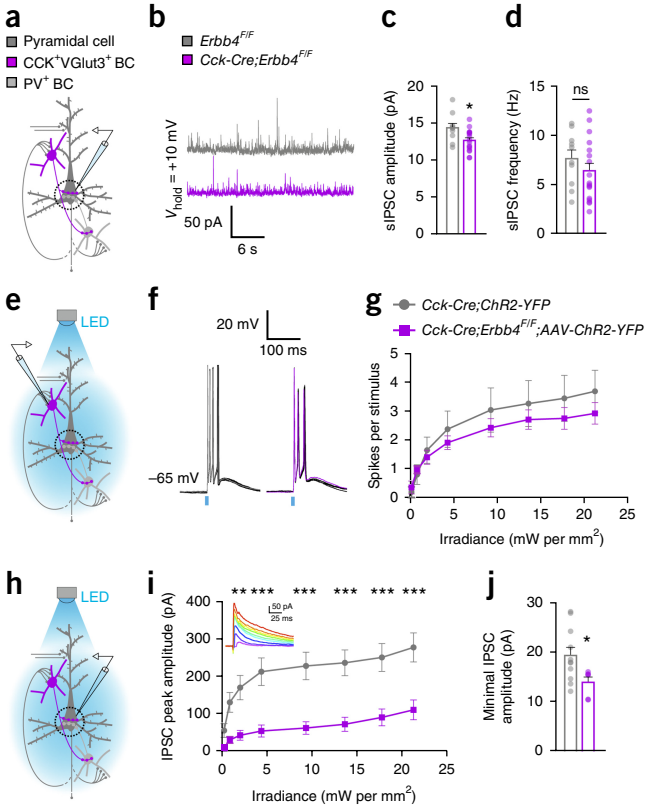

Figure 3 Functional impairment of inhibition in CA1 pyramidal cells of *Cck-Cre;Erbb4*$^{F/F}$ mice at P60–70. (**a**) Scheme of *Erbb4* deletion from CCK$^+$ interneurons. The circle indicates the recording site. (**b–d**) sIPSC sample traces (**b**), mean sIPSC amplitude (**c**) and mean sIPSC frequency (**d**) in pyramidal neurons. V_{hold}, holding voltage. *t* test, $t_{(25)} = 2.646$, $^*P = 0.015$; $t_{(25)} = 1.03$, $P = 0.313$ (ns, not significant), $n = 10$ and 17 neurons from 3 control and 6 mutant mice, respectively. (**e**) Schematic of experiment configuration. (**f**) CCK$^+$ interneurons in *Cck-Cre* and *Cck-Cre;Erbb4*$^{F/F}$ mice fire multiple action potentials in response to full-field optogenetic stimulation (1-ms, 473-nm LED flash). (**g**) Spikes fired per stimulus, as a function of irradiance. Two-way ANOVA, $F_{(8, 72)} = 14.65$, $P < 0.001$; the two groups do not differ significantly in their response to photostimulation, two-way ANOVA genotype effect, $F_{(8, 72)} = 14.65$, $P = 0.150$; interaction effect, $F_{(8, 72)} = 0.357$, $P = 0.939$; $n = 5$ cells in each group. (**h**) Schematic of experiment configuration. (**i**) Effects for photostimulation irradiances on the peak amplitude of evoked IPSCs. Two-way ANOVA, genotype effect, $F_{(1, 189)} = 102.3$, $^{**}P = 0.0046$, $^{***}P < 0.001$. Two-way ANOVA, interaction effect, $F_{(8, 182)} = 1.532$, $P = 0.149$, $n = 11$ and 12 neurons from 5 control and 5 mutant mice, respectively. Multiple comparison testing (Sidak's test) revealed significant differences at 2 mW/mm^2 irradiance and above. (**j**) Minimal optogenetic stimulation to evoke IPSCs, Mann–Whitney test, $U = 12$, $P = 0.034$, $n = 11$ and 6 neurons from 5 control and 4 mutant mice, respectively. Data are expressed as mean ± s.e.m.

for a novel object were similar for the two genotypes in both tests (**Fig. 5c–f**). In object location tasks, however, conditional mutants were less capable of discriminating a displaced object than control mice, independently of the retention interval (**Fig. 5d,f**). These experiments suggest that the impaired wiring and function of CCK$^+$VGlut3$^+$ interneurons do not interfere with recognition memory in general, but disrupt the ability of conditional mutants to recognize new spatial configurations, a task that is critically dependent on hippocampal function[30,31].

To investigate to what extent spatial information encoding is affected in *Cck-Cre;Erbb4*$^{F/F}$ mutant mice, we assessed spatial reference

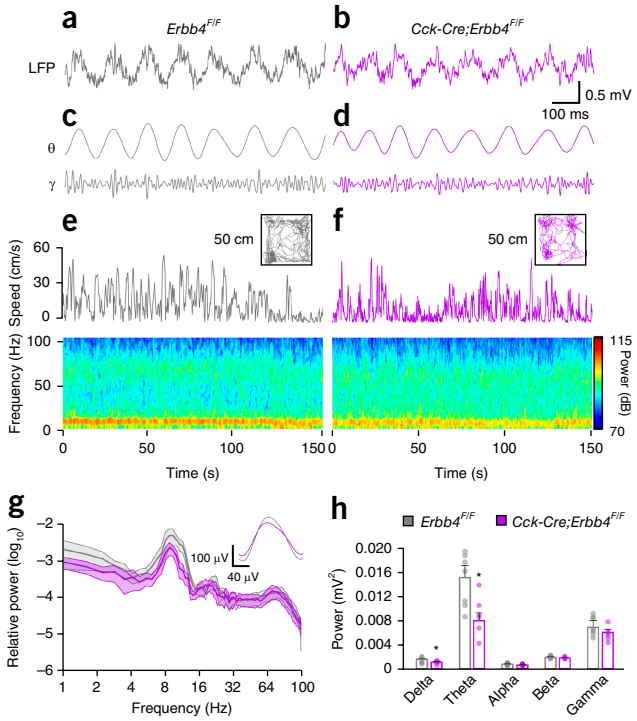

Figure 4 Disturbed hippocampal oscillatory activity in *Erbb4* conditional mutant mice in hippocampal CA1. (**a**,**b**) Spontaneous LFPs from control (**a**) and mutant (**b**) mice. Epochs in which animals were moving at a speed above 5 cm/s were selected to obtain LFP epochs during similar behaviors. (**c**,**d**) Filtered LFP signal in the theta and gamma bands (top and bottom traces, respectively). (**e**,**f**) Spontaneous exploration: instantaneous speed (top) for depicted open fields (50 × 50 cm) and spectrograms (bottom) for control (**e**) and mutant (**f**) mice. (**g**) Power spectrum of CA1 LFP from 0.5–100 Hz in control and mutant mice. The inset depicts the mean theta cycle in control and mutant mice. (**h**) CA1 LFP band-power in the delta (0.5–4 Hz), theta (4–12 Hz), alpha (13–15 Hz), beta (16–30 Hz) and gamma (31–100 Hz) frequency bands. *t* test, delta $t_{(11)} = 2.23$, $^*P = 0.047$; theta $t_{(11)} = 2.815$, $^*P = 0.016$, alpha $t(11) = 2.09$, $P = 0.059$; beta $t_{(11)} = 0.61$, $P = 0.55$, gamma $t_{(11)} = 0.42$, $P = 0.45$, $n = 7$ control and 6 mutant mice. Data are expressed as mean ± s.e.m.

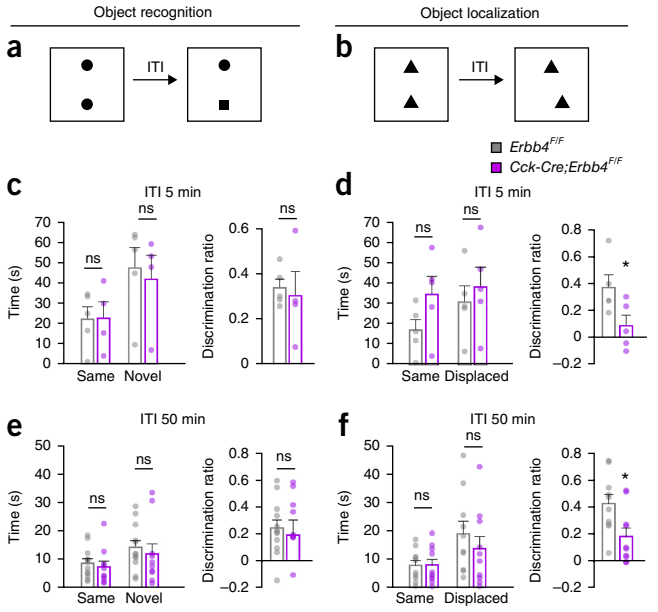

Figure 5 Deficits in recognition of spatial novelty in *Erbb4* conditional mutant mice. (**a**,**b**) Schemes of novel object (**a**) and object-place (**b**) recognition tasks. (**c**–**f**) Time spent with the two objects during the test phase and discrimination index for novel object recognition (**c**,**e**) and object-place (**d**,**f**) recognition tasks. From left to right: (**c**) *t* test, $t_{(7)} = 0.05023$, $P = 0.9613$, $t_{(7)} = 0.3631$, $P = 0.7272$, $t_{(8)} = 0.341$, $P = 0.743$, $n = 5$ control and 4 mutant; (**d**) *t* test, $t_{(8)} = 1.704$, $P = 0.1269$, $t_{(8)} = 0.5873$, $P = 0.5732$, $t_{(8)} = 2.321$, $^*P = 0.049$, $n = 5$ control and 5 mutant; (**e**) *t* test, $t_{(20)} = 0.5142$, $P = 0.6127$, $t_{(20)} = 0.5671$, $P = 0.5769$, $t_{(20)} = 0.439$, $P = 0.665$, $n = 12$ control and 10 mutant; (**f**) *t* test, $t_{(18)} = 0.04202$, $P = 0.9669$, $t_{(18)} = 0.8552$, $P = 0.4037$, $t_{(18)} = 2.603$, $^*P = 0.018$, $n = 10$ control and 10 mutant. ITI, inter-trial interval; ns, not significant. Data are expressed as mean ± s.e.m.

memory using the Morris water maze (MWM). The acquisition phase and the probe test analysis failed to reveal prominent differences between the two genotypes (**Supplementary Fig. 12a–f**). However, closer examination revealed that whereas control mice switched from thigmotaxis to full exploration of the maze on the second day, *Cck-Cre;Erbb4*$^{F/F}$ mutant mice shifted to full exploratory behavior 1 d later (**Fig. 6a**,**b**). This observation suggested that conditional mutants might have a delay in spatial learning.

To further explore spatial memory, we used the eight-arm radial maze. We first carried out experiments in a conventional version of the radial maze (three of eight arms baited, all arms remaining open), simultaneously assessing reference and working memory (**Supplementary Fig. 12g–i**). In this task, reference memory errors (entries into an unbaited arm) and total errors (reference errors plus entries into already visited arms) were higher and showed significance ($P = 0.0178$ and $P = 0.0242$, respectively) at day 3 in *Cck-Cre;Erbb4*$^{F/F}$ mutants compared to controls (**Supplementary Fig. 12g**,**h**). In contrast, working memory errors (re-entries into an arm) were not significantly different ($P = 0.1339$) between controls and their mutant littermates (**Supplementary Fig. 12i**), which indicated that working memory might not be particularly affected in these mutants. Consistently, we did not observe prominent differences between controls and mutants in other working memory tests (**Supplementary Fig. 11b**,**c**).

We used two different automated eight-arm radial maze setups to further characterize memory impairments in *Cck-Cre;Erbb4*$^{F/F}$ mutants (**Fig. 6c**,**f**). We analyzed reference memory again by using a radial-maze task (with three of eight arms baited) in which re-entries were prevented. As in the MWM, *Cck-Cre;Erbb4*$^{F/F}$ mutants showed a transitory delay of spatial learning (**Fig. 6c**,**d**). In contrast, long-term retention of spatial memory was not altered; mutant mice even made fewer errors than controls in the retention test (**Fig. 6c**,**e**). Then we evaluated short-term working memory with an experimental design that allowed us to manipulate the task demands on retention (which arm was visited last) and organization (update of successive spatial memories, avoiding interference from irrelevant memories) by using different inter-trial intervals (see Online Methods and ref. 32). *Cck-Cre;Erbb4*$^{F/F}$ mutants showed a selective impairment in the organization but not the retention aspects of spatial short-term memory (**Fig. 6f–h**). These findings indicate that abnormal wiring and function of CCK$^+$VGlut3$^+$ interneurons do not affect short-term or working memory in general, but selectively disrupt an organizational component necessary for the fast update of spatial memories. Collectively, our experiments demonstrate that *Cck-Cre;Erbb4*$^{F/F}$ mice display deficits in hippocampus-dependent learning tasks that require encoding of spatial information and update of new spatial information during short-term memory, but can consolidate and retrieve spatial information normally.

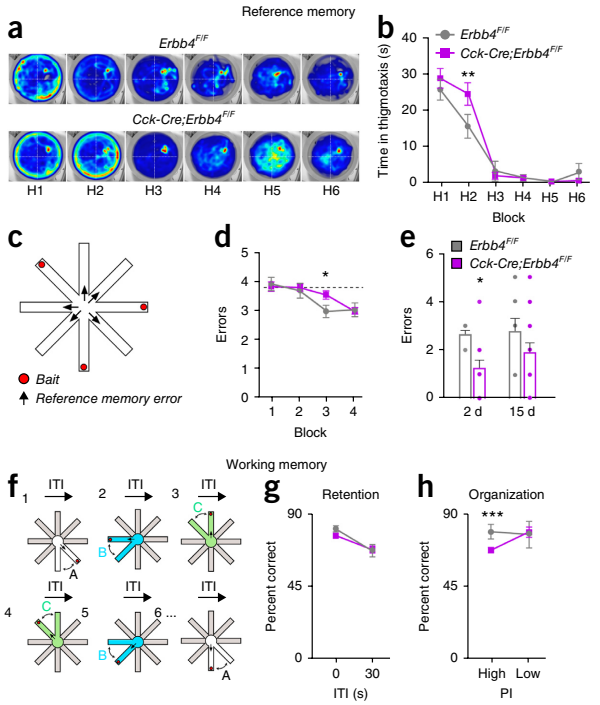

Figure 6 Delayed acquisition of spatial reference memory and deficits in hippocampal spatial organization in *Erbb4* conditional mutant mice. (**a**,**b**) Mice were trained in the MWM for 6 d (H1–H6) to find a submerged platform located in the center of the NE quadrant. (**a**) Heat maps representing the average distribution for a group of tracks from control (top) and *Cre;Erbb4*$^{F/F}$ mutant groups (bottom), $n = 8$ control and 17 mutant mice. Color is mapped to the range of location frequencies in each heat map separately (blue minimum and red maximum per-pixel frequency). (**b**) Time spent navigating the outer diameter of the tank during the MWM. Two-way repeated measurements ANOVA with Fisher's least significant difference (LSD) for multiple comparisons, $t_{(138)} = 2.963$, $^{**}P = 0.0036$, $n = 8$ control and 17 mutant mice. (**c**) Schematic of experiment configuration for the reference memory test in an automated eight-arm radial maze. (**d**) Learning curve for reference memory test in the automated eight-arm radial maze. Each block corresponds to the average of 2 d training. Two-way ANOVA, time effect $F_{(3, 69)} = 9.873$, $P < 0.001$, $n = 8$ control and 17 mutant mice. Controls reached performance under chance level during the third block; *Cre;Erbb4*$^{F/F}$ mutant mice, not until 2 d later. Two-way ANOVA with Fisher's LSD for multiple comparisons, $t_{(92)} = 2.224$, $^{*}P = 0.0286$, $n = 8$ control and 17 mutant mice. (**e**) Long-term memory retrieval test 2 and 15 d after the reference memory training. Genotype effect, two-way ANOVA $F_{(1, 23)} = 5.711$, $^{*}P = 0.0254$. *Cck-Cre;Erbb4*$^{F/F}$ mutant mice made significantly fewer reference memory errors 2 d after training but not 15 d after training. Two-way ANOVA with Fisher's LSD for multiple comparisons, 2 d $t_{(46)} = 2.218$, $^{*}P = 0.0315$, 15 d $t_{(46)} = 1.385$, $P = 0.1727$, $n = 8$ control and 17 mutant mice. (**f**) Schematic of experiment configuration for the working memory test in an automated eight-arm radial maze. In a different radial maze setup and after 2 d of habituation, mice were trained to alternate between three different pairs of arms presented in pseudorandom order. (**g**) Percentage correct alternations performed by control and *Cre;Erbb4*$^{F/F}$ mutant mice in sessions with high or low memory retention demand. Both groups scored higher at 0 s inter-trial interval (ITI) than at 30 s ITI. Two-way ANOVA with Fisher's LSD for multiple comparisons, $F_{(1, 23)} = 19.941$, $P = 0.0002$; genotype effect $F_{(1, 23)} = 0.511$, $P = 0.4819$; interaction effect $F_{(1, 23)} = 0.993$, $P = 0.3295$; $n = 8$ control and 17 mutant mice. (**h**) Percentage correct alternation in trials with high or low hippocampal organization and proactive interference (PI) demand. PI × genotype interaction effect two-way ANOVA with Fisher's LSD, $F_{(1, 23)} = 5.389$, $P = 0.0295$. *Cck-Cre;Erbb4*$^{F/F}$ mutant mice made significantly fewer correct choices only under high PI, two-way ANOVA with Fisher's LSD for multiple comparisons, $F_{(1,23)} = 14.475$, $^{***}P < 0.001$, $n = 8$ control and 17 mutant mice. Data are expressed as mean ± s.e.m.

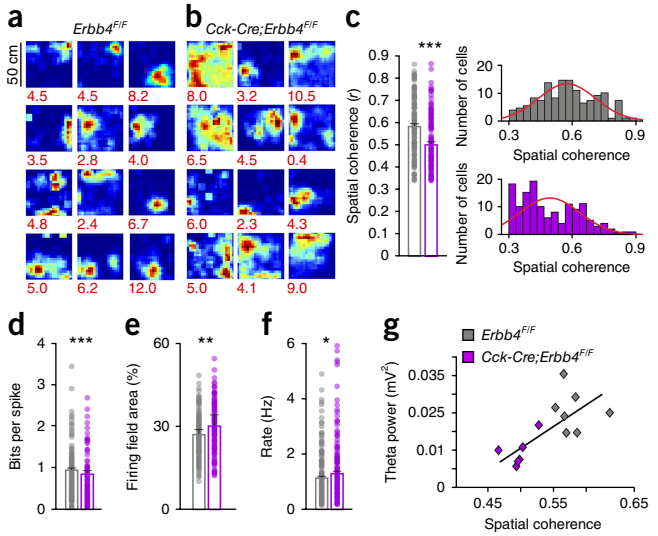

Figure 7 Impaired spatial representation by place cells in the hippocampus of *Erbb4* conditional mutant mice. (**a**,**b**) Firing-rate maps showing the discharge of representative control (**a**) and mutant (**b**) place cells. Firing fields are organized following centrality and dispersion values for the distribution in each group. Values at the bottom of each firing map indicate the maximal firing rate (red). (**c**) Left, spatial coherence values for control and mutant mice. Right, distributions of spatial coherences for place cells in control and mutant mice. Mann–Whitney, $U = 6{,}540$, $^{***}P < 0.001$; $n = 147$ and 131 neurons from 7 control and 6 mutant mice, respectively. (**d**–**f**) Mean values for spatial information (Mann–Whitney, $U = 6{,}551$, $^{***}P < 0.001$), firing fields (*t*-test, $t_{(276)} = -2.75$, $^{**}P = 0.006$) and firing rates (Mann–Whitney, $U = 8{,}309.5$, $^{*}P = 0.048$), $n = 147$ and 131 neurons from 7 control and 6 mutant mice. (**g**) Correlation between theta power and the spatial coherence of place cells, Pearson, $r = 0.707$, $^{**}P = 0.006$. Data are expressed as mean ± s.e.m.

Defective place cells fields in CCK-specific *Erbb4* mutants

The previous results prompted us to investigate the characteristics of place cells in *Cck-Cre;Erbb4*$^{F/F}$ conditional mutants. We implanted tetrodes in the hippocampus and recorded the activity of single units during a pellet-chasing exploration task in the open field. We isolated single units from these recordings and selected those that met specific qualitative and quantitative criteria for place cells (see Online Methods and **Supplementary Figs. 13** and **14**). Most pyramidal cells displayed spatial selectivity in control mice, but not in *Cck-Cre;Erbb4*$^{F/F}$ conditional mutants (**Fig. 7a**,**b**). Detailed analyses revealed that single units in the mutants had lower spatial coherence and spatial information per spike than in controls (**Fig. 7c**,**d**). In contrast, we found that the firing field area and firing rates of pyramidal neurons were greater in *Cck-Cre;Erbb4*$^{F/F}$ mutants than in controls (**Fig. 7e**,**f**). As in our findings during spontaneous exploration (**Fig. 4**), we found a decrease in theta power between the two groups, with no changes in theta/delta ratio or theta mean frequency (data not shown). To assess whether the distortion of theta activity could predict place cells properties, we correlated the theta power obtained during the pellet-chasing task with the mean spatial coherence. We found a significant correlation between the two parameters (**Fig. 7g**).

To investigate the stability of place cells in *Cck-Cre;Erbb4*$^{F/F}$ mutant mice, we divided baseline recordings into two epochs and determined pairwise correlations between the firing rate maps for each cell within the same recording session (intra-trial). Place cell stability was significantly lower in conditional mutants than in controls (**Fig. 8a**–**c**). Consistently, we also found a higher percentage of unstable place cells in *Cck-Cre;Erbb4*$^{F/F}$ mutants than in controls (**Fig. 8d**). In contrast,

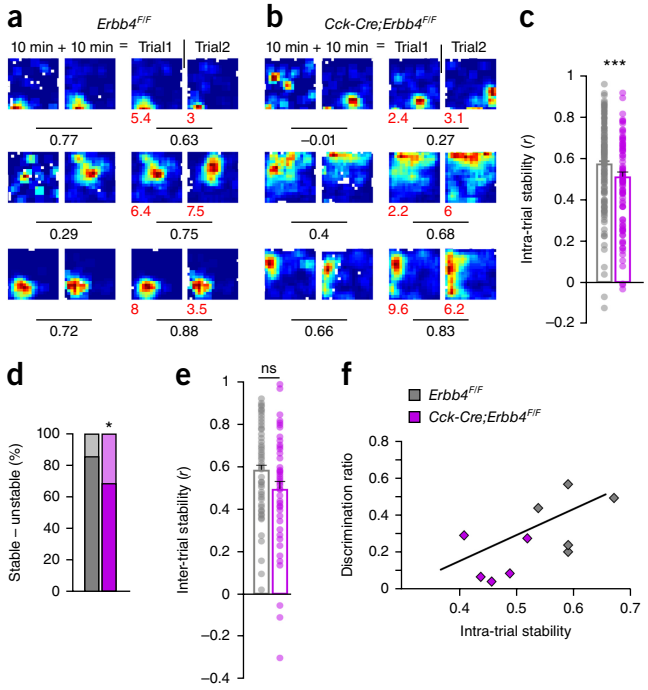

Figure 8 Abnormal stability of place cells in *Erbb4* conditional mutant mice. (**a**,**b**) Representative firing-rate maps for control (**a**) and mutant (**b**) place cells. For each genotype, the first two columns illustrate firing-rate maps for the same 20-min trial, with the first column displaying the first 10 min of the trial and the second column the second 10 min of the trial. Columns three and four show firing rates for two different 20-min trials (trial 1 and trial 2) separated by 5 min. Values show maximum firing rate (red) and spatial coherence (black). Values under lines represent the spatial correlation between firing maps above. (**c**) Intra-trial stability, Mann–Whitney test, $U = 4{,}948$, $^{***}P < 0.001$, $n = 147$ and 99 cells from 7 controls and 6 mutants, respectively. (**d**) Percentage of stable and remapping units, $\chi^2_{(1)} = 6.31$, $^{*}P = 0.012$. (**e**) Inter-trial stability, Mann–Whitney test, $U = 1{,}075$, $P = 0.054$ (ns, not significant), $n = 51$ and 53 cells from 4 controls and 5 mutants, respectively. (**f**) Performance in the spatial object recognition was correlated with the intra-trial stability of place cells, Pearson, $r = 0.640$, $^{*}P = 0.046$, $n = 106$ and 118 cells from 5 controls and 5 mutants, respectively. Data are expressed as mean ± s.e.m.

stability across different recording sessions (inter-trial) was not significantly different between the two genotypes (**Fig. 8e**). We also noticed that intra-trial stability strongly correlated with performance in the object-place recognition task, which suggests that the behavioral abnormalities might be linked to place cell stability (**Fig. 8f**). Taken together, our results indicated that place cells exhibit lower spatial modulation in *Cck-Cre;Erbb4*$^{F/F}$ mutants than in controls, which reveals a prominent role for CCK$^+$VGlut3$^+$ interneurons in circuits processing novel spatial configurations.

DISCUSSION

Understanding the effect that specific classes of GABAergic interneurons have on cortical operations is essential to understanding the organization of cortical microcircuits. The function of interneurons is largely determined by their spiking properties, synaptic features and specific connectivity, but little is known about the molecular mechanisms that regulate these processes for different classes of interneuron. Here we identified ErbB4 as an essential regulator of the wiring of CCK$^+$VGlut3$^+$ interneurons, a population of basket cells whose contribution to cortical function has remained elusive. Genetic manipulation of the normal connectivity of CCK$^+$VGlut3$^+$ interneurons revealed a critical role for these cells in the regulation of theta oscillatory activity and in the coding of spatial information in the hippocampus. Our findings thus demonstrate that normal integration of CCK$^+$VGlut3$^+$ interneurons in cortical circuits is required for accurate spatial representations of the environment.

ErbB4 is required for the wiring of CCK$^+$VGlut3$^+$ basket cells

The fine-tuning of cortical networks is orchestrated by a collection of interneuron classes with distinctive neurochemical and electrophysiological properties and, most notably, axonal targets. Since the location of synaptic contacts largely determines the influence of interneurons on the postsynaptic neuron, it has been suggested that the elaborate organization of inhibitory inputs greatly increases the overall computational power of individual neurons[3]. Basket cells comprise a major group of interneurons whose synapses surround the cell body and proximal dendrites of their postsynaptic targets, and they therefore constitute particularly powerful regulators of the firing of principal cells[33]. The two main classes of basket cells, PV$^+$ fast-spiking and CCK$^+$ regular-spiking basket cells, are distinctly wired in cortical circuits[34]. Previous studies have shown that PV$^+$ cells require ErbB4 to develop and maintain a normal number of excitatory inputs[14,16–18]. Here we found that ErbB4 signaling is also required for the development of a normal complement of excitatory synapses in CCK$^+$ basket cells, which suggests that at least some of the mechanisms controlling the wiring of basket cells are shared. In contrast, while PV$^+$ basket cells do not seem to require ErbB4 to make synapses onto pyramidal cells[16,18], we found that loss of ErbB4 in CCK$^+$ basket cells prominently decreased the number of synapses that these cells make and impaired their ability to inhibit pyramidal cells. This finding is consistent with electron microscopy findings that ErbB4 is present in about a quarter of the inhibitory synapses contacting the somata of pyramidal cells[14].

Abnormal wiring of CCK$^+$VGlut3$^+$ basket cells disrupts theta oscillations

Different classes of cortical interneurons seem to contribute to information processing by timing the activity of specific neural networks and gating information flow in relation to specific behavioral states[2,3]. The introduction of new genetic means that provide unprecedented targeting specificity, together with the tools to manipulate interneuron activity *in vivo*, is greatly accelerating progress in the field[9,10,35–37]. Genetic manipulation of CCK$^+$ interneurons, however, has proven difficult because CCK is also abundantly expressed in pyramidal cells[23,38]. Due to the selective expression of ErbB4 in GABAergic cells[14,19], *Cck-Cre;Erbb4*$^{F/F}$ conditional mutants represent a unique resource for examining the contribution of CCK$^+$VGlut3$^+$ basket cells to cortical operations. While the developmental nature of the genetic manipulation reported here might lead to deficits that are not directly comparable to those might be expected during the acute probing of CCK$^+$VGlut3$^+$ basket cells, our study offers important clues to the function of these interneurons.

Previous studies have shown that CCK$^+$ basket cells in the hippocampus fire on the ascending theta phase, when pyramidal cell assemblies emerge[21,39]. Conversely, these interneurons are weakly coupled to gamma oscillations in anesthetized rats[39]. In *Cck-Cre;Erbb4*$^{F/F}$ conditional mutants, abnormal wiring of CCK$^+$VGlut3$^+$ basket cells led to decreased power of low-frequency oscillations in freely moving animals during exploration, with no significant changes in gamma frequency. These deficits are likely due to defects in cortical CCK$^+$VGlut3$^+$ basket cells, as none of the main subcortical generators

of theta activity—medial septum, pedunculopontine tegmentum and raphe nuclei[28,29]—are targeted in *Cck-Cre* mice. In contrast, CA1-projecting neurons in the entorhinal cortex are strongly innervated by CCK$^+$VGlut3$^+$ basket cells[40], and so it is possible that defects in entorhinal CCK$^+$VGlut3$^+$ basket cells may also contribute to the phenotype described here.

CCK$^+$VGlut3$^+$ basket cells and spatial coding

Most hippocampal pyramidal cells discharge at very low frequency during spatial navigation, but when the animal enters into the place field of a specific unit, this neuron increase its firing more than a hundred times[41]. It has been hypothesized that CCK$^+$ basket cells are well suited to enhancing this contrast in firing rate during theta oscillations through a form of short-term plasticity called depolarization-induced suppression of inhibition[42]. This involves the selective suppression of inhibition specifically in the terminals of CCK$^+$ interneurons innervating the active place cell, while CCK$^+$ interneurons continue to release GABA to the majority of the silent pyramidal cells. This process is mediated by the spatially restricted action of endocannabinoids released by the active place cell, which act on CCK$^+$ interneurons through presynaptic CB1 receptors[22,25]. Our analysis suggests that defective wiring of CCK$^+$VGlut3$^+$ basket cells leads to abnormal firing fields for place cells in *Cck-Cre;Erbb4$^{F/F}$* mutants. It is tempting to speculate that these defects are caused by the failure of CCK$^+$VGlut3$^+$ basket cells to suppress the activity of neighboring pyramidal cells outside the field of the place cell. In addition, the reduced inhibitory control over PV$^+$ interneurons observed in *Cck-Cre;Erbb4$^{F/F}$* mutants may also contribute to the decreased spatial coherence and stability of place cells, as modulation of PV$^+$ activity is linked to the precision of hippocampal spatial representations by place cells and, indeed, perisomatic inhibition is very effective in regulating spike timing[37,43]. Alternatively, a potential alteration of synaptic weights across different subpopulations of cells might alter the necessary temporal dynamics for a stable spatial representation and other memory processes, including spatial remapping. We cannot rule out the possibility that deficits in CCK$^+$ErbB4$^+$ interneurons in the entorhinal cortex and other parahippocampal regions contribute to the stability of the place cells[44]. In any case, our results reinforce the notion that CCK$^+$ interneurons modulate spatial coding by pyramidal place cells.

Our conclusions are reinforced by the observation that abnormal wiring of CCK$^+$VGlut3$^+$ basket cells led to important hippocampus-dependent behavioral alterations. *Cck-Cre;Erbb4$^{F/F}$* conditional mutants exhibited severe deficits in the object location test, which requires fast encoding, and in the radial maze working memory task with maximized organization demand, which requires fast encoding and updating of spatial memories[32,45]. At least some of these deficits are due to defective hippocampal function, as bilateral lesions in the entorhinal cortex do not affect object location tasks[46] and the function of place cells has been linked to novelty associated with an object location[47,48]. We cannot exclude the possibility, however, that abnormal function of CCK$^+$VGlut3$^+$ basket cells in other cortical areas contributes to some extent to the deficient coding of spatial information in the hippocampus and therefore to the behavioral abnormalities observed in *Cck-Cre;Erbb4$^{F/F}$* conditional mutants. Considering the links that exist between ErbB4 signaling and psychiatric disorders[49], it will be interesting to explore how alterations in CCK interneurons might contribute to the pathophysiology of neurodevelopmental disorders.

METHODS

Methods, including statements of data availability and any associated accession codes and references, are available in the online version of the paper.

Note: Any Supplementary Information and Source Data files are available in the online version of the paper.

ACKNOWLEDGMENTS

We are very thankful to C. Garcia-Frigola for scientific advice and support, M. Fernández, D. Baeza and V. Rodríguez-Millán for technical assistance, T. Gil and F. Navarrete for lab support, and J.Z. Huang (Cold Spring Harbor Laboratory) for mouse colonies (*Cck-Cre* and *VIP-Cre*). We thank C. Fernandes for guidance during an early phase of behavioral experiments at King's College London, S. Al Abed for technical advice and stimulating discussions on behavioral experiments performed at the Magendie Institute, and C. Leteneur for help with the behavioral experiments. We are grateful to L. Menéndez de la Prida and M. Maravall for critically reading early versions of this manuscript, and members of the Marín and Rico laboratories for stimulating discussions and ideas. Supported by grants from Fundación Alicia Koplowitz and the European Research Council (ERC-2012-StG 310021) to B.R., from the European Research Council (ERC-2011-AdG 293683) to O.M., from the Spanish Government (CONSOLIDER CSD2007-00023) and Lilly Research Awards Program to B.R. and O.M, and from the French government (ANR-10-EQX-008-1 to A.M. and LabEX BRAIN ANR-10-LABX-43 to A.F. and A.M.). O.M. and B.R. are Wellcome Trust Investigators.

AUTHOR CONTRIBUTIONS

I.d.P. performed cell, synaptic, biochemical and behavior experiments and analyzed data. J.R.B.-M. performed *in vivo* electrophysiology recordings and analyzed data. A.M.-S. carried out *in vitro* electrophysiology recordings and analyzed data. A.M. contributed to the behavior analysis. A.F. contribute with resources. I.d.P., O.M. and B.R. wrote the manuscript.

COMPETING FINANCIAL INTERESTS

The authors declare no competing financial interests.

1. Ascoli, G.A. *et al.* Petilla terminology: nomenclature of features of GABAergic interneurons of the cerebral cortex. *Nat. Rev. Neurosci.* **9**, 557–568 (2008).
2. Kepecs, A. & Fishell, G. Interneuron cell types are fit to function. *Nature* **505**, 318–326 (2014).
3. Klausberger, T. & Somogyi, P. Neuronal diversity and temporal dynamics: the unity of hippocampal circuit operations. *Science* **321**, 53–57 (2008).
4. Bartos, M. & Elgueta, C. Functional characteristics of parvalbumin- and cholecystokinin-expressing basket cells. *J. Physiol. (Lond.)* **590**, 669–681 (2012).
5. Freund, T.F. & Katona, I. Perisomatic inhibition. *Neuron* **56**, 33–42 (2007).
6. Tricoire, L. *et al.* A blueprint for the spatiotemporal origins of mouse hippocampal interneuron diversity. *J. Neurosci.* **31**, 10948–10970 (2011).
7. Somogyi, J. *et al.* GABAergic basket cells expressing cholecystokinin contain vesicular glutamate transporter type 3 (VGLUT3) in their synaptic terminals in hippocampus and isocortex of the rat. *Eur. J. Neurosci.* **19**, 552–569 (2004).
8. Valero, M. *et al.* Determinants of different deep and superficial CA1 pyramidal cell dynamics during sharp-wave ripples. *Nat. Neurosci.* **18**, 1281–1290 (2015).
9. Cardin, J.A. *et al.* Driving fast-spiking cells induces gamma rhythm and controls sensory responses. *Nature* **459**, 663–667 (2009).
10. Sohal, V.S., Zhang, F., Yizhar, O. & Deisseroth, K. Parvalbumin neurons and gamma rhythms enhance cortical circuit performance. *Nature* **459**, 698–702 (2009).
11. Hefft, S. & Jonas, P. Asynchronous GABA release generates long-lasting inhibition at a hippocampal interneuron-principal neuron synapse. *Nat. Neurosci.* **8**, 1319–1328 (2005).
12. Daw, M.I., Tricoire, L., Erdelyi, F., Szabo, G. & McBain, C.J. Asynchronous transmitter release from cholecystokinin-containing inhibitory interneurons is widespread and target-cell independent. *J. Neurosci.* **29**, 11112–11122 (2009).
13. Chattopadhyaya, B., Baho, E., Huang, Z.J., Schachner, M. & Di Cristo, G. Neural cell adhesion molecule-mediated Fyn activation promotes GABAergic synapse maturation in postnatal mouse cortex. *J. Neurosci.* **33**, 5957–5968 (2013).
14. Fazzari, P. *et al.* Control of cortical GABA circuitry development by Nrg1 and ErbB4 signalling. *Nature* **464**, 1376–1380 (2010).
15. Neddens, J. & Buonanno, A. Selective populations of hippocampal interneurons express ErbB4 and their number and distribution is altered in ErbB4 knockout mice. *Hippocampus* **20**, 724–744 (2010).
16. Del Pino, I. *et al.* Erbb4 deletion from fast-spiking interneurons causes schizophrenia-like phenotypes. *Neuron* **79**, 1152–1168 (2013).

17. Ting, A.K. *et al.* Neuregulin 1 promotes excitatory synapse development and function in GABAergic interneurons. *J. Neurosci.* **31**, 15–25 (2011).
18. Yang, J.M. *et al.* Development of GABA circuitry of fast-spiking basket interneurons in the medial prefrontal cortex of erbb4-mutant mice. *J. Neurosci.* **33**, 19724–19733 (2013).
19. Vullhorst, D. *et al.* Selective expression of ErbB4 in interneurons, but not pyramidal cells, of the rodent hippocampus. *J. Neurosci.* **29**, 12255–12264 (2009).
20. Földy, C., Malenka, R.C. & Südhof, T.C. Autism-associated neuroligin-3 mutations commonly disrupt tonic endocannabinoid signaling. *Neuron* **78**, 498–509 (2013).
21. Klausberger, T. *et al.* Complementary roles of cholecystokinin- and parvalbumin-expressing GABAergic neurons in hippocampal network oscillations. *J. Neurosci.* **25**, 9782–9793 (2005).
22. Neu, A., Földy, C. & Soltesz, I. Postsynaptic origin of CB1-dependent tonic inhibition of GABA release at cholecystokinin-positive basket cell to pyramidal cell synapses in the CA1 region of the rat hippocampus. *J. Physiol. (Lond.)* **578**, 233–247 (2007).
23. Taniguchi, H. *et al.* A resource of Cre driver lines for genetic targeting of GABAergic neurons in cerebral cortex. *Neuron* **71**, 995–1013 (2011).
24. Golub, M.S., Germann, S.L. & Lloyd, K.C. Behavioral characteristics of a nervous system-specific erbB4 knock-out mouse. *Behav. Brain Res.* **153**, 159–170 (2004).
25. Katona, I. *et al.* Presynaptically located CB1 cannabinoid receptors regulate GABA release from axon terminals of specific hippocampal interneurons. *J. Neurosci.* **19**, 4544–4558 (1999).
26. Fish, K.N., Sweet, R.A. & Lewis, D.A. Differential distribution of proteins regulating GABA synthesis and reuptake in axon boutons of subpopulations of cortical interneurons. *Cereb. Cortex* **21**, 2450–2460 (2011).
27. Raastad, M., Storm, J.F. & Andersen, P. Putative single quantum and single fibre excitatory postsynaptic currents show similar amplitude range and variability in rat hippocampal slices. *Eur. J. Neurosci.* **4**, 113–117 (1992).
28. Gogolák, G., Stumpf, C., Petsche, H. & Sterc, J. The firing pattern of septal neurons and the form of the hippocampal theta wave. *Brain Res.* **7**, 201–207 (1968).
29. Vertes, R.P., Colom, L.V., Fortin, W.J. & Bland, B.H. Brainstem sites for the carbachol elicitation of the hippocampal theta rhythm in the rat. *Exp. Brain Res.* **96**, 419–429 (1993).
30. Save, E., Poucet, B., Foreman, N. & Buhot, M.C. Object exploration and reactions to spatial and nonspatial changes in hooded rats following damage to parietal cortex or hippocampal formation. *Behav. Neurosci.* **106**, 447–456 (1992).
31. Stupien, G., Florian, C. & Roullet, P. Involvement of the hippocampal CA3-region in acquisition and in memory consolidation of spatial but not in object information in mice. *Neurobiol. Learn. Mem.* **80**, 32–41 (2003).
32. Al Abed, A.S. *et al.* Estradiol enhances retention but not organization of hippocampus-dependent memory in intact male mice. *Psychoneuroendocrinology* **69**, 77–89 (2016).
33. Armstrong, C. & Soltesz, I. Basket cell dichotomy in microcircuit function. *J. Physiol. (Lond.)* **590**, 683–694 (2012).
34. Mátyás, F., Freund, T.F. & Gulyás, A.I. Convergence of excitatory and inhibitory inputs onto CCK-containing basket cells in the CA1 area of the rat hippocampus. *Eur. J. Neurosci.* **19**, 1243–1256 (2004).
35. Lee, S., Kruglikov, I., Huang, Z.J., Fishell, G. & Rudy, B. A disinhibitory circuit mediates motor integration in the somatosensory cortex. *Nat. Neurosci.* **16**, 1662–1670 (2013).
36. Pfeffer, C.K., Xue, M., He, M., Huang, Z.J. & Scanziani, M. Inhibition of inhibition in visual cortex: the logic of connections between molecularly distinct interneurons. *Nat. Neurosci.* **16**, 1068–1076 (2013).
37. Royer, S. *et al.* Control of timing, rate and bursts of hippocampal place cells by dendritic and somatic inhibition. *Nat. Neurosci.* **15**, 769–775 (2012).
38. Burgunder, J.M. & Young, W.S. III. Cortical neurons expressing the cholecystokinin gene in the rat: distribution in the adult brain, ontogeny, and some of their projections. *J. Comp. Neurol.* **300**, 26–46 (1990).
39. Lasztóczi, B., Tukker, J.J., Somogyi, P. & Klausberger, T. Terminal field and firing selectivity of cholecystokinin-expressing interneurons in the hippocampal CA3 area. *J. Neurosci.* **31**, 18073–18093 (2011).
40. Varga, C., Lee, S.Y. & Soltesz, I. Target-selective GABAergic control of entorhinal cortex output. *Nat. Neurosci.* **13**, 822–824 (2010).
41. O'Keefe, J. Place units in the hippocampus of the freely moving rat. *Exp. Neurol.* **51**, 78–109 (1976).
42. Freund, T.F., Katona, I. & Piomelli, D. Role of endogenous cannabinoids in synaptic signaling. *Physiol. Rev.* **83**, 1017–1066 (2003).
43. Korotkova, T., Fuchs, E.C., Ponomarenko, A., von Engelhardt, J. & Monyer, H. NMDA receptor ablation on parvalbumin-positive interneurons impairs hippocampal synchrony, spatial representations, and working memory. *Neuron* **68**, 557–569 (2010).
44. Fyhn, M., Hafting, T., Treves, A., Moser, M.B. & Moser, E.I. Hippocampal remapping and grid realignment in entorhinal cortex. *Nature* **446**, 190–194 (2007).
45. Mingaud, F. *et al.* Retinoid hyposignaling contributes to aging-related decline in hippocampal function in short-term/working memory organization and long-term declarative memory encoding in mice. *J. Neurosci.* **28**, 279–291 (2008).
46. Hales, J.B. *et al.* Medial entorhinal cortex lesions only partially disrupt hippocampal place cells and hippocampus-dependent place memory. *Cell Rep.* **9**, 893–901 (2014).
47. Kim, J., Delcasso, S. & Lee, I. Neural correlates of object-in-place learning in hippocampus and prefrontal cortex. *J. Neurosci.* **31**, 16991–17006 (2011).
48. Larkin, M.C., Lykken, C., Tye, L.D., Wickelgren, J.G. & Frank, L.M. Hippocampal output area CA1 broadcasts a generalized novelty signal during an object-place recognition task. *Hippocampus* **24**, 773–783 (2014).
49. Mei, L. & Nave, K.A. Neuregulin-ERBB signaling in the nervous system and neuropsychiatric diseases. *Neuron* **83**, 27–49 (2014).

ONLINE METHODS

Mice. Mice were maintained in a C57B/6 background. *Cck-Cre;Erbb4$^{F/F}$* mice were generated by breeding *Cck-Cre* mice[23] with mice carrying *loxP*-flanked (*F*) *Erbb4* alleles[24]. *VIP-Cre* (ref. 23), *RCE* (Jackson Laboratory 032037)[50] and *Ai9/tdTomato* lines (Jackson Laboratory 007905)[51] were used for expression analysis. In some experiments, control mice included mice carrying wild-type and *Cck-Cre* alleles. All animal procedures were approved by the ethics committee (UMH-CSIC, Spain and Home Office, UK) and met the guidelines of the local and European regulations and the standards for use of laboratory animals.

Immunohistochemistry and *in situ* hybridization. For immunohistochemistry, adult (P30 and P60) mice were transcardially perfused and brains postfixed for 2 h. Immunohistochemistry was performed in 40-µm-thick sections as described previously[14]. Primary antibodies used: mouse anti-β-galactosidase (1:500, Promega #Z3781), anti-ErbB4 (1:300; Thermo Scientific #MA5-12888, specificity tested in the *HER4^{heart};Erbb4$^{-/-}$* mouse), anti-GAD65 (1:500; Millipore #MAB351R), anti-NeuN (1:500; Millipore #MAB377), anti-parvalbumin (1:500; Sigma #P-3088), anti-PSD95 (1:500; NeuroMab #70-028); rabbit anti-CCK8 (1:300; Immunostar #20078), anti-ErbB4 0618 (1:300, a gift from C. Lai)[14], anti-parvalbumin (1:500; Swant #PV-25), anti-VGlut3 (1:500, Synaptic Systems #135203), anti-VIP (1:1,000; Immunostar #20077); guinea pig anti-VGlut1 (1:2,000; Chemicon #AB5905), anti-VGlut3 (1:500; Frontier Institute, #NM153725); goat anti-CB1 (1:500; Frontier Institute #Af450-1) and anti-ChAT (1:100; Chemicon #AB144p); chicken anti-GFP (1:1,000; Aves Lab #1020). Secondary antibodies and Alexa-conjugated streptavidin were purchased from Molecular Probes (#A-11034, #A-31572, #A-11039, #A-11029, #A-31570, #A-11055, #S21381), Jackson (#706-065-148, #715-175-150) or Vector (BA-1000). For the reconstruction of neurobiotin-filled axons and staining of VGlut3 boutons, we used a modified protocol described before[52]. Briefly, 300-µm sections used for patch-clamp electrophysiology were incubated overnight with 555-streptavidin (1:100; Molecular Probes) and the primary and the secondary antibodies were incubated for 48 h and overnight, respectively, at 4 °C. For standard *in situ* hybridization, brains were postfixed overnight in 4% PFA and 20-µm sections were hybridized with digoxigenin-conjugated probes as described previously[53]. cDNA probes were cloned from adult (P30) cortical cDNA into the pCRII-Topo vector (Sigma) using the primers described in the Allen Mouse Brain Atlas.

Imaging and quantification. Images were acquired at 8-bit depth and 1,024 × 1,024 pixel resolution in an inverted Leica TCS-SP8 confocal microscope. For cell colocalization analyses, images were acquired with a 40×, 1.4 NA objective and 0.75 digital zoom at 400 Hz. For synaptic bouton and cluster analysis, images were acquired with a 100×, 1.44 NA objective and 2.2 digital zoom at 200 Hz. Analysis of synaptic bouton and cluster densities was performed blind to genotype using Fiji (ImageJ) software as described previously[16]. For double-positive bouton analysis, the binaries for both channels were overlaid and those particles ≥ 0.2 µm^2 in the colocalization mask were filtered as double-positive CB1$^+$VGlut3$^+$ boutons. For cell density analysis, CCK and VGlut3 cells were quantified on 40-µm brain sections using Neurolucida software. CCK is also expressed in pyramidal cells, which precludes the quantification of CCK$^+$ interneurons located in the pyramidal cell layer using this technique. To overcome this problem, and given that pyramidal cells seemed to express lower levels of CCK mRNA than interneurons, we carried out experiments with a short exposure to the colorimetric reaction. By doing that, we were able to clearly identify putative CCK$^+$ interneurons in the stratum pyramidale, stratum radiatum and stratum oriens. To confirm that we were detecting most interneurons, we also carry out experiments with a longer exposure. At least in the stratum radiatum and oriens, the density of CCK$^+$ cells was the same with short or long exposures to the reaction. For the assessment of axonal synaptic density, we first identified the neurobiotin-positive, VGlut3-positive neurons and followed their axons. Axons were distinguished by their small diameter, tortuosity and presence of bouton-like varicosities. We confirmed that bouton-like varicosities contained VGlut3 staining. Then we restricted our quantification to neurobiotin-filled varicosities, since VGlut3 staining in the varicosities decreased as the axon penetrated deeper into the tissue. Confocal images were taken using a 100×, 1.4 NA objective and Neurolucida software was used for the analysis. Density of varicosities was normalized to a 100-µm segment of axon length in those CCK-cells in which more than 100 µm of axon could be followed in the slice.

Western blot. Samples were prepared from P30 control and *Cck-Cre;Erbb4$^{F/F}$* hippocampi homogenized in lysis buffer containing 50 mM Tris pH7.5, 150 mM NaCl, 5 mM EDTA, 1% Triton X-100, 0.5 mM pervanadate with Protease Inhibitor Cocktail (Complete, Mini, Roche). Samples were denatured and run on 10% SDS–PAGE gels. Polyacrylamide gels were electrophoretically transferred onto PVDF membranes (Whatman GmbH). Membranes were blocked with 5% BSA (Sigma) in TBS (20 mM Tris-HCl, pH7.5, 150 mM NaCl) for 1h and probed with primary antibodies: anti-βIII-tubulin (1:2,000; Sigma #T8660), anti-GAD65 (1:1,000; Millipore #MAB351R) and anti-GAD67 (1:1,000; Chemicon #MAB5406), in 1% BSA in TBS plus 0.1% Tween20. Subsequently, they were treated with horseradish-peroxidase-conjugated secondary antibodies (1:5,000, Pierce, #31444) and ECL western blotting detection reagents (Immobilon, Millipore). Signals were acquired as 16-bit images with a luminescence image analyzer (LAS-1000PLUS; Fujifilm) and quantified with Quantity One 1D analysis software (Bio-Rad Laboratories).

Stereotaxic injections. Adeno-associated viruses containing pAAV-DIO:EF1α:hChR2 (H134R)-EYFP:WPRE:hGHpA (a gift from K. Deisseroth, Stanford University, and produced commercially by UNC Vector, serotype AAV2/1 at 4 × 10^{12} IFU/ml) were delivered bilaterally to the hippocampus of adult (P60–70) *Cck-Cre* or *Cck-Cre;Erbb4$^{F/F}$* mice anesthetized with isoflurane by stereotaxic injection using pulled glass pipettes. In brief, glass pipettes were back-filled and then placed in a Nanoliter2010 injector and front-filled with virus. Animals were anesthetized in an induction chamber with 5% isoflurane for 3 min, head-fixed in a stereotaxic frame and then maintained at 1.5–2.5% isoflurane. The stereotaxic coordinates to target bilaterally both dorsal and ventral CA1 subfields were as follows: A/P, −2.3; M/L, ±1.5; D/V, −1.2; and A/P, −3.2; M/L, ±3.8; D/V, 2.5 (from bregma). Volume (110 nl at each stereotaxic coordinate) and speed (75 nl/min) of the injections were controlled by a WPI Micro4 pump. The pipette was retracted from the brain after a 5-min waiting period to allow diffusion. After suturing and disinfecting with Betadine, mice were injected with 100 µl of buprenorphine 0.03 mg/ml) and allowed to recover for 2–4 weeks before *in vitro* electrophysiology experiments.

***In vitro* patch clamp recordings.** P60–70 mice were deeply anesthetized with sodium pentobarbital and transcardially perfused with ice-cold *N*-methyl-D-glucamine (NMDG)-based cutting solution, containing (in mM) 93 NMDG, 2.5 KCl, 1.2, NaH_2PO_4, 30 $NaHCO_3$, 20 HEPES, 25 glucose, 5 sodium ascorbate, 2 thiourea, 3 sodium pyruvate, 10 $MgSO_4$, 0.5 $CaCl_2$, adjusted to pH 7.3 with HCl. After brain dissection, 300 µm transverse hippocampal slices were cut using a vibratome (Leica) in the same ice-cold NMDG-based solution. After cutting, slices were allowed to recover for 15 min at 33 °C. Slices were then transferred to holding artificial cerebrospinal fluid (hACSF) at room temperature, where they were incubated for an additional 45 min and then throughout the day before recording. hACSF contained (in mM) 92 NaCl, 2.5 KCl, 1.2 NaH_2PO_4, 30 $NaHCO_3$, 20 HEPES, 25 glucose, 5 sodium ascorbate, 2 thiourea, 3 sodium pyruvate, 2 $MgSO_4$, 2 $CaCl_2$.

Patch clamp recordings. Slices were transferred to a chamber continuously superfused with recording ACSF (rACSF) heated to 34 °C. rACSF contained (in mM) 127 NaCl, 2.5 KCl, 0.6 NaH_2PO_4, 26 $NaHCO_3$, 13 glucose, 1.3 $MgSO_4$, 2 $CaCl_2$. Pyramidal neurons (stratum pyramidale) or putative CCK interneurons (stratum radiatum) from hippocampal CA1 areas were viewed with infrared differential interference optics (Hamamatsu camera controller) through a 40× water-immersion objective (Olympus). Patch microelectrodes (4–8 MΩ) were pulled from borosilicate glass (1.5 mm outer diameter × 0.86 mm inner diameter; Harvard Apparatus) using a vertical P10 puller (Narishige).

Voltage clamp recordings. To measure sIPSCs, sEPSCs and evoked IPSCs, we used a cesium-based intracellular solution containing (in mM) 135 cesium methanesulfonate, 8 KCl, 10 HEPES, 4 Mg-ATP, 0.4 Na-GTP, 5 QX-314, 0.1 spermine, 0.5 EGTA. Cells were kept under current-clamp or voltage-clamp configuration with an Axoclamp 200A amplifier operating in fast mode. Data were filtered online at 2 kHz and acquired at a 20-kHz sampling rate using pClamp 6.0.2 software (Molecular Devices). Spontaneous events were analyzed using Mini-Analysis (Synaptosoft) and current clamp recordings were analyzed with Clampfit 10.2.

In vitro optogenetics. All optogenetic experiments were conducted under 40 µM D-APV and 40 µM CNQX (Tocris). Photostimulation consisted of full-field flashes (1 ms, 0.2 Hz) delivered by TTL square-pulse activation of a Cool LED

doi:10.1038/nn.4544

light source (473 nm) through a 40× water-immersion objective (Olympus), with the field of view centered in the middle of stratum radiatum directly beneath or above the recorded cell, respectively, for pyramidal or CCK interneuron recordings. Photostimulation intensity at the slice was systematically varied between 0.05 mW/mm^2 and 21.2 mW/mm^2, with 10–20 trials recorded per stimulation intensity. Recordings were targeted to EYFP-rich areas of CA1, indicating recombination of the conditional EYFP-ChR2 vector. Optogenetically evoked spikes were recorded in fluorescently labeled CCK interneurons in stratum radiatum under current-clamp (in mM, 130 gluconate, 5 KCl, 10 HEPES, 2 $MgCl_2$, 10 sodium phosphocreatine, 2 Na_2-ATP and 0.4 Na-GTP) in order to allow neurobiotin (1 mg/ml) labeling and postrecording confirmation of CCK immunoreactivity. Current–voltage curves for ChR2 photocurrents were obtained by recording from ChR2-expressing CA1 pyramidal neurons under voltage clamp in the presence of 40 μM D-APV and CNQX, as well as 20 μM gabazine (Tocris). Optogenetically evoked IPSCs were recorded from pyramidal neurons in voltage clamp at a holding potential (+10 mV) that resulted in exclusively negative direct photocurrents, with 10 μM AM-251 being used to prevent depolarization-induced suppression of inhibition[54]. Evoked IPSCs were detected within a 50-ms time window after stimulus onset and the peak amplitude of the earliest IPSC was measured. Evoked IPSCs were readily distinguishable from spontaneous events due to their predictable and reliable trial-to-trial latency after stimulus onset. For minimal stimulation experiments, photostimulation intensity was reduced until no IPSCs could be evoked. At this point, stimulation intensity was increased until a combination of failures and consistent-amplitude IPSCs could be observed. Under our experimental conditions this transition was sharp, with most cells showing a change from 0 to 60–70% successful trials within a 0.03 mW/mm^2 increment in irradiance.

Behavioral analysis. Behavioral studies were performed with male adult (P60) mutant mice and control littermates. Mice were housed in standard cages in a 12-h dark/light cycle. Water and rodent chow were available *ad libitum* during all tests with the exception of the rewarded alternation test. All tests were performed during the light phase of the light/dark cycle by trained observer blind to genotype. The open field, object recognition, Y maze, elevated plus maze and dark/light box were videotaped using a computer-assisted data acquisition system (Smart, PANLAB, Spain). With the exception of the sequential object recognition task[48], all behavioral tests were separated at least by 24 h. The order of tests were as follows: open field, object recognition, spontaneous alternation in Y maze, elevated plus maze, rewarded alternation in T maze, dark-light box, PPI. Two additional batches of ungenotyped mice were tested exclusively in spatial learning and memory related tasks, using a classical automated radial maze (EthoVision) and a water maze using a computer-assisted tracking system (Imetronic or Viewpoint), and genotyped following the last behavioral task.

Open field and habituation. The open field consisted of a white acrylic glass arena of 48 × 48 × 30 cm under uniform lightning conditions 25 lux. Mice were allowed to explore the arena for 10 min. The arena was delimited into two regions using the SMART software: zone 1, the central square area of 25 × 25 cm equidistant from the walls, and zone 2, the remaining borders. The time spent, velocity as well as transitions between the two zones was monitored as explained above. Habituation to the open field was performed 4 d after first exposure to the arena under the same conditions as described before.

Novel object recognition task. The object recognition task was performed under the same environmental conditions as in the open field. During the training session, mice were allowed to individually explore two objects for 10 min and time spent exploring each object was recorded. Then mice were returned to the home cage and the open field and object were cleaned to avoid olfactory cues. After an inter-trial interval of 50 min, the mouse was placed back into the same open field in which one of the familiar objects had been replaced by a novel object. The mice did not show any object preference before trials. Mice were excluded from the analysis only if the total time of exploration for each mouse was lower than 5 s in the test session. Object exploration was defined as the mouse being within 2 cm of an object, directing its nose at the object, and being involved in active exploration such as sniffing. A discrimination index (I_d) was calculated to measure recognition memory:

$$I_d = \frac{\left(t_{\text{new object}} - t_{\text{familiar object}}\right)}{\left(t_{\text{new object}} + t_{\text{familiar object}}\right)}$$

Spatial object recognition task. Object-place recognition task was performed in the same environmental conditions as the open field. During the training session, mice were allowed to explore for 10 min two identical objects placed in parallel in the center of the arena at 10 cm of the open field walls. Between the training and test session the mice were placed back into their home cage and the arena as well as objects were cleaned to avoid olfactory cues. After a 50 min delay, one object randomly selected was displaced 10 cm away from its previous position in the arena in a random direction but keeping the same distance to the closest wall, and during the test phase, mice were allowed to explore for an additional 10 min. Mice were excluded from the analysis only if the total time of exploration for each mouse was lower than 5 s in the test session. A discrimination index (I_d) was calculated to measure recognition memory:

$$I_d = \frac{\left(t_{\text{displaced object}} - t_{\text{undisplaced object}}\right)}{\left(t_{\text{displaced object}} + t_{\text{undisplaced object}}\right)}$$

Sequential object and object-place recognition task. To exclude a possible phenotype in novel/displaced object recognition due to the session block when the tasks were performed, a combination of object and object-place recognition tasks was performed sequentially on the same day similarly to the model described before[48]. Mice were allowed to explore two objects in the arena twice for 10 min. Then a spatial object recognition task was performed, displacing an object 10 cm away from its previous position in the arena, and exploration was recorded for 10 min. Finally, one of the familiar objects were substituted by a novel object and exploration was allowed and recorded for another 10 min. During all trials, an inter-trial interval of 5 min was applied during which the animals where placed back into their home cage and the objects as well as the arena were cleaned. The objects were presented and displaced in a counterbalanced order to avoid spontaneous object preference.

Morris water maze (MWM). Testing was performed in a circular tub of 150 cm diameter filled with opaque liquid (21 °C water rendered opaque by a nontoxic white cosmetic adjuvant) as previously described[55]. Mice were trained to swim to a submerged platform (14 cm diameter, 1 cm below the water surface) using visual cues placed distally (at least 1 m from the maze walls) on black curtains surrounding the maze. Data were collected with a video camera fixed to the room's ceiling and connected to a computerized tracking system (Viewpoint) located in an adjacent room. To assess performance, the escape latency, distance to the target, time spent on thigmotaxis, and swim speed were analyzed as outcome measures for each session with EthoVision XT software (Noldus).

In the acquisition training, mice were trained for two daily trials with a cutoff of 60 s. Once on the platform, they were allowed to remain on it 10 s. When mice did not find the platform, the experimenter led them to it. The platform was placed in the middle of the NE quadrant and mice were released randomly from different starting points (NW, SW or SE) facing the wall.

In the probe testing, the probe trials were designed to examine the extent of spatial discrimination learning at the end of the last day of acquisition training. To achieve this, the platform was removed from the pool and the mice were allowed to navigate for 60 s. The percentage of distance that the mice spent exploring the target quadrant (where the platform was located during the hidden platform training) was measured over the 60 s trial.

In the allocentric navigation test, we assayed after the probe test whether mice were using the visual cues to locate the platform. To test this, all distal cues and platform were rotated in the same direction one quadrant and mice were allowed to find the platform during 60 s.

Classical eight-arm radial maze. A fully open eight-arm radial maze was used to assess for both working and reference memory using a single task. The classical eight-arm radial maze was made of a transparent Plexiglas maze with 22 cm long and 7 cm wide radial arms with 20 cm high walls. The maze was located in a sound proof room with white walls and a constant illumination of 60 lux. Distal visual cues of different colors, shapes and volumes were placed on the walls at 1 m distance from the center maze. Mice were weighted daily and food was progressively restricted (small chow pieces of 1.5–2.5 g given to each mouse, depending on body weight loss), to maintain 85–90% of the free-feeding body weight throughout the experiment. Habituation to the maze was performed during the 2 d before the test. For assessment of spatial reference and working memory, the bait (dry milk pellets) was placed in three arms (1, 2 and 4) and the mice were

allowed to freely explore until they collected all the three baits. Mice performed two trials a day and the maze was cleaned between each trial. Every day, the maze was rotated randomly 45, 90 or 180° to dissociate potential intra-maze cues from the distal cues and surrounding environment. In addition, at the end of each arm, a false bottom was filled with the bait to keep mice from performing spatial entries guided by the bait's odor. Following Olton's definition, entries into an arm that has been visited previously constituted working memory errors, whereas entries into an arm that is never baited constitute a reference memory error.

Working memory test, memory retention and interference assessment in an automated radial maze. We used three fully automated eight-arm radial maze made of gray Plexiglas (Imetronic, Pessac, France), as described before[32,45]. Mice were food deprived as previously described for the classical eight-arm radial maze and habituated during the 2 d before the working memory training, as described before[32]. Working memory test started the following day. We used a working memory task designed to assess mnemonic retention and organization and update of spatial information as previously described[32,45]. Mice are assigned six arms grouped into three pairs (A, B, C) and must concomitantly store different pieces of spatial information related to three different events[32]: the last visited arm in each. Each training session consisted of a pseudorandom presentation of the arm pairs (20 trials for each session). The location of the food varied according to an alternation rule in each arm: every time arm pair A is opened, the bait is loaded into the last nonvisited arm. Mice remember which arm of a given pair is visited in the last trial until the next presentation of the same pair takes place. This task requires the mouse to retain the memory of the last visited arm in each pair of arms independently and update this stored information for each of them to alternate its choices between the two arms of each pair across repetitions. To assess memory retention and organization, three sessions were performed with different inter-trial intervals (ITI) between the presentations of the pairs of arms (0 s and 30 s ITI). The task therefore requires retaining in memory the last arm visited in any given trial n within one of the three pairs (the sampling trial) until the next trial within that same pair, $n + 1$ (the testing trial). Performance under low or high retention demand was assessed by using a short (0 s) or long (30 s) ITI, respectively. This task also requires organization of spatial information to overcome interference between repetitions in order not to confuse the n trial with the previous one within the same pair $n - 1$ (the proactively interfering trial). Thus, the organizational difficulty of the trials depends on the proactive interference, determined by the proximity between the sampling trial n and the proactively interfering trial $n - 1$. Within each of the 0 s ITI testing conditions, trials with low versus high proactive interference (PI) levels were distinguished. High interference occurs when a presentation of a pair of arms has been performed with 1 or fewer presentations of other pairs in between (0 or 1 intervening trials). This results in a more frequent presentation of the pair and requires the last spatial location visited by the animal to be updated in shorter time (high proactive interference). Low interference occurs when the presentation of the pair of arms is separated by 2–4 trials in other pairs, therefore requiring an update more spaced in time.

Reference memory test in an automated radial maze. This task is designed to specifically assess reference memory, the ability to acquire a cognitive map—that is, spatial information stable in time about the general layout of a particular environment. The reference memory task took place in a new room with an automated eight-arm radial maze setup not explored previously (technical description described above). Animals were deprived as previously described and habituated to the new radial maze setup to collect all baits from the eight arms. The task to assess reference memory consisted of baiting consistently three out of eight arms separated by 90 and 135° (arms 1, 3 and 6). Mice performed two trials per day. For each trial they were allowed to explore each arm for a single time only until the three baits were collected. Closing the arm automatically after the visit prevented re-entries. Learning criterion was achieved when the average of number of errors for each group was under the chance level (number of errors at chance = 3.79 when, of 8 arms, 3 are correct and 5 count as an error). For long-term memory retrieval, mice were left in the housing room for 2 or 15 d with rodent chow *ad libitum*. They were food restricted 12–16 h before the beginning of the memory retrieval test. Reference memory retrieval test consisted of a single trial.

Spontaneous alternation task in a Y maze. Testing was carried out in a transparent Y maze (arms 40 cm long were 7 cm wide × 15 cm high, spaced at 120 degrees from each other). Mice were placed into the center of the maze and allowed to freely explore for 8 min. The sequence of mouse entries was recorded. Entries in each arm were counted only if 100% of mouse body including the tail passed into maze's arm. The alternation behavior was quantified as described before[16].

Rewarded alternation task in a T maze. Spatial working memory was assessed with a rewarded alternation task on a continuous black T maze under the same environmental conditions as before but with distal spatial cues. Before the pre-training period animals were habituated for 8 min to a black T maze (70 cm long × 50 cm wide, enclosed by walls 15 cm high). Light sources in the room were adjusted to provide the same light intensity in every arm of the maze (25 lux). Chocolate milk was used as a reward and was fed in the home cages the same day of habituation to avoid hyponeophagia. After habituation, mice were food deprived as previously described for the classical eight-arm radial maze. Then animals were pretrained daily to the T maze until the consumption of the reward reached 80%. For spatial nonmatching to place testing, each trial consisted of a sample run and a choice run as described before[43]. Learning the alternation task was performed with 20 randomized left–right trials or to a maximum time of 50 min per animal. Mice were tested in a counterbalanced order and an interval of 10 s was set between sample and choice runs. Criterion point for a correct trial was that the whole animal (including tip of the tail) entered the rewarded arm. The maze was cleaned between trials to avoid any potential odor cues. Mice selected for the statistical analysis were those reaching 80% alternation at the end of the training period.

Elevated plus maze. As in previous work[16], the plus maze consisted of four arms (50 × 10 cm) elevated 50 cm above the floor: two enclosed arms with black acrylic glass walls (30 cm high) and two open (wall-free) arms joined through a central platform (10 × 10 cm). Indirect illumination provided 60 lux onto the open arms and 15 lux onto the closed arms. Mice were place in the center of the maze facing a closed arm and their behavior was recorded and tracked for 5 min with a camera above the maze coupled to the Smart tracking system (PANLAB, Spain). This allowed for automated assessments of the time spent and the number of entries in the different compartments.

Dark/light box. The dark/light box test is aimed at assessing anxiety behavior. This test is based on the innate aversion of mice to avoid strongly illuminated areas and on the spontaneous exploratory behavior of rodents in response to a novel environment[56]. We used two boxes of the same size (25 × 25 cm): one open box with direct illumination of 170 lux (light box) and an opaque black acrylic box (dark box). Mice were placed facing the dark box and their behavior was recorded for 10 min and video tracked in the light box. Time spent in the light box as well as number of transitions between the two chambers was quantified.

Prepulse inhibition (PPI). Startle responses and inhibition of startle responses after presentation of a nonstartling pulse (prepulse) was measured in an animal acoustic startle response system (Harvard Apparatus) as described before[57]. Mice were habituated to a transparent plastic restrainer and to the conditioning chamber without background noise twice for 8 min the day before the PPI test. Presentation of acoustic pulse and prepulse stimuli was controlled by the Startle interface (Harvard Apparatus) which recorded the responses from the accelerometer. The test session consisted of a 5-min acclimatization period to a background noise at 70 dB followed by three 20-ms initial pulse stimuli at 120 dB to determine the initial amplitude of the acoustic startle response. Test sessions consisted of four different trial types presented 12 times in a pseudorandom order at a 7–23 s inter-trial variable interval: pulse-only stimulus of 120 dB and three different 20-ms prepulse trials of 10, 15 and 20 dB above the background noise (70 dB) followed by a 20-ms startle pulse of 120 dB 100 ms later. The average value for each type of trial across the twelve blocks was used to calculate the percentage PPI using the following formula:

$$\%\mathrm{PPI} = 100\left(\frac{\text{startle amplitude in pulse trial} - \text{startle amplitude in prepulse trial}}{\text{startle amplitude in pulse trial}}\right)$$

***In vivo* recordings on freely moving mice.** Eight control and ten mutant male mice between 60 and 90 d of age were implanted with micro-drives (Axona) with four independent screws loaded with tetrodes (12 µm tungsten wire, California Fine Wire Company, Grover Beach, CA, USA). Electrodes were implanted under isoflurane anesthesia and buprenorphine analgesia through a craniotomy above the hippocampus of control and *Cck-Cre;Erbb4*$^{F/F}$ mutant male mice as described before[16]. Recordings were performed between 60 and 120 d of age. Animals with misplaced electrodes or showing lesions were omitted from the analysis. No statistical methods were used to predetermine sample sizes, but our sample sizes

doi:10.1038/nn.4544

are similar to those reported in our previous publications. Data collection and analysis were not performed blind to the conditions of the experiment.

Data acquisition. As in previously studies[16,58], electrophysiological recordings were obtained using 16-channel head stage (gain ×1), with an infrared light-emitting diode (LED) to track mouse position (Axona Ltd, UK). Signals were amplified (400 to 1,000 times), band-pass filtered (0.3 Hz to 24 kHz, Dacq system, Axona, UK) and recorded at 48 kHz with 24-bit precision. These recordings were initially used to determine electrode location before the implementation of the recording protocols. For single-unit recordings, signal was band-pass filtered between 380 Hz and 6 kHz. Spikes were recorded whenever the signal was 3–4 times above background noise, typically 20–30 μV, and stored in windows of 1 ms duration (200 ms before threshold and 800 ms after threshold detection). The same channels were also recorded in continuous mode at a frequency of 4.8 kHz and band-pass filtered between 0.3 and 2.4 kHz.

Local field potential recordings. During recording sessions, animals were examined for basal activity while they were in their home cages. Tetrodes were lowered until typical hippocampal activity was observed. Ripple power, unit activity and theta power were used as electrophysiological landmarks to determine electrode location. Recordings were performed in the pyramidal cell layer of CA1 of the hippocampus. Anteroposterior and mediolateral coordinates were similar in all animals. Dorsoventral location was verified to be in the CA1 pyramidal cell layer by the presence of flat ripples. Then mice were placed in a black square area (50 cm × 50 cm) made of Plexiglas and recorded while freely exploring for 20 min. For experimental homogeneity, data included for band power analysis and theta-gamma relationship were obtained during the first exploratory session in the open field. To correlate spatial coherence with theta power, we used LFP recordings obtained during the pellet-chasing experiments.

Place cells recordings. Animals were food-deprived to 85–90% of their original weight before recording sessions. Small pellets of food were thrown in every 20 s to random locations in the open field, keeping the animal in continuous locomotion, thereby allowing a complete sampling of the environment. For sequential object and object-place recognition task in implanted animals, a similar pellet-chasing paradigm was followed and mice underwent the same object recognition test previously described[48].

Data analysis. Local field potentials and firing rate maps were analyzed using Cronux (code available at http://chronux.org/) and custom-written Matlab (MathWorks, Natick, MA, USA) code, respectively (available as **Supplementary Software 1–5**; updates of scripts on reasonable request). Raw recordings were FIR filtered (<1.2 kHz) and downsampled to 2.4 kHz. As in previous work[16], data obtained in the open field recordings were used to characterize the local field potential. Running speed was computed based on the coordinates of the animal's position and epochs above 5 cm/s were included for analysis, obtaining epochs of similar behaviors in the two groups. To visualize the power spectrum in relationship to the speed of movement, the spectral power (in decibels, $10 \cdot \log_{10}$) and spectrogram were built using the Thomson multi-taper method. Then a sliding window with 50% overlap, yielding a frequency resolution of 1 Hz, was used. For group comparisons, periodograms were plotted and the power (mV^2) for different bands was calculated and then filtered by epochs in which the speed was above 5 cm/s as described before[16]. Complementary analysis was performed to eliminate delta-related artifacts but include all behavioral states. We carried out a segmentation of the LFP in windows of 1 s and included, for the analysis, epochs in which the theta/delta ratio was above 3. We confirmed that theta power was significantly lower in the *Cck-Cre;Erbb4*$^{F/F}$ mice.

Unit isolation. Single-unit activity was isolated using cluster cutting techniques developed for data acquired with tetrodes, TINT (Axona, St. Albans, UK). Principal components, peak–trough distance, voltage at time *t*, peak height, trough, time of peak and time of trough in each electrode were used for unit isolation. Klustakwik was used for initial discrimination of clusters and manual refinement was performed using principal components, spike amplitude and other parameters. To verify cluster quality isolation, the probability of cluster overlapping was calculated as described before[59,60] (**Supplementary Fig. 13**). Spike trains were analyzed by generating interval time histograms and a temporal autocorrelogram (**Supplementary Fig. 14**). Only units with no spikes in the refractory period of the inter-spike time histogram (1–2 ms) and with spike amplitudes 3–4 times above background noise, typically 20–30 μV, were included. Putative pyramidal cells and interneurons were differentiated following previous criteria[58,60] (**Supplementary Fig. 13**).

Firing rate maps. Matlab (MathWorks, Natick, MA, USA) code (available as **Supplementary Software 1–5**; updates of scripts on reasonable request) were developed for place cell activity analysis. Firing-rate maps were assembled as described previously[58,61]. Pixel maps were converted to a bin matrix with a bin size of 2.5 cm × 2.5 cm (**Supplementary Fig. 13**). Firing rate in each bin was determined by a smoothing process using overlapping squares of 7.5 cm × 7.5 cm as described before[58,62]. Firing fields were plotted as a contour map reflecting the frequency of firing; colors were interpolated from the top firing bins down to the lowest by scaling them in decreasing intervals of peak firing and assigning a color scale: red for highest frequency, dark blue for lowest.

The spatial information content was quantified using the Skaggs information index over the smoothed map[62]. This index calculates the spatial information per spike:

$$I = \sum_i P_i \left(\lambda_i / \lambda\right) \log_2 \left(\lambda_i / \lambda\right)$$

where λ_i is the mean firing rate in bin *i*, λ is the overall mean firing rate and P_i is the occupancy probability of bin *i*.

Spatial coherence is a spatial autocorrelation measurement from which a correlation coefficient is calculated between the rate for each bin and the average rate of the eight surrounding bins . Firing fields were defined as a group of at least six contiguous bins where the firing frequency was above the mean firing rate plus the standard error of the firing matrix. The maximal firing frequency of this group of bins was required to be above 1 Hz. For those units displaying more than one firing field, firing field size was computed as the sum of the existing firing fields and expressed as the percentage of the arena size occupied by the firing field, calculated using the smoothed firing matrix. In-field maximum frequency was computed as the maximum firing field frequency of the smoothed firing map. Mean frequency was computed as the total number of spikes divided by the total recording time to provide the average session firing rate expressed in Hz.

To classify units as having spatially related activity, a randomized distribution was calculated using the values obtained in the original unsmoothed firing map and respecting the position matrix (n = 1,000). Although we observed low spatial information per spike in some of the place cells selected, we verified that the spatial coherence obtained from the original map compared with the randomized distribution was the most efficient strategy to determine spatial firing on single-cell basis. Thus, for a unit to be regarded as being spatially modulated, cells had to display a spatial coherence above 99% of the randomized distribution[58]. This same random distribution was used to obtain a stability index between the original and a random distribution. To determine the spatial stability of place cells during the intra-trial comparison and across different trials, we only compared units recorded during trials in which the at least the 70% of the arena was covered. Thus, for units to be regarded as stable they had to be above 99% of the cross-correlation between the original and the randomized distribution (**Supplementary Fig. 14**).

Statistics. SPSS software (IBM Corp) was used for statistical analysis and all data are presented as mean ± s.e.m. Biological replicates (n values are different populations derived from different brains from different litters) were analyzed to assess biological variability and reproducibility of data. In general, no statistical methods were used to predetermine sample sizes but chosen sample sizes were similar to those reported in previous publications[16] or to those generally employed in the field. No randomization was used. Differences were considered significant when $P < 0.05$. To obtain unbiased data, experimental mice from both genotypes were processed together and quantifications were performed blinded to the genotype. Data was analyzed with parametric tests, *t* test or ANOVA, when data sets met assumptions of normality (Kolmogorov–Smirnov test) and homoscedasticity (Levene test). Non-parametric tests for independent groups, Mann-Whitney and χ^2 tests were applied when normality was not met or when comparing probability distributions.

A **Supplementary Methods Checklist** is available.

Data and code availability. Custom code is available as **Supplementary Software 1–5** and on reasonable request. The data that support the findings of this study are available from the corresponding authors upon reasonable request.

50. Soriano, P. Generalized lacZ expression with the ROSA26 Cre reporter strain. *Nat. Genet.* **21**, 70–71 (1999).
51. Madisen, L. *et al.* A robust and high-throughput Cre reporting and characterization system for the whole mouse brain. *Nat. Neurosci.* **13**, 133–140 (2010).
52. Fogarty, M.J., Hammond, L.A., Kanjhan, R., Bellingham, M.C. & Noakes, P.G. A method for the three-dimensional reconstruction of Neurobiotin™-filled neurons and the location of their synaptic inputs. *Front. Neural Circuits* **7**, 153 (2013).
53. Flames, N. *et al.* Delineation of multiple subpallial progenitor domains by the combinatorial expression of transcriptional codes. *J. Neurosci.* **27**, 9682–9695 (2007).
54. Földy, C., Neu, A., Jones, M.V. & Soltesz, I. Presynaptic, activity-dependent modulation of cannabinoid type 1 receptor-mediated inhibition of GABA release. *J. Neurosci.* **26**, 1465–1469 (2006).
55. Moreau, M.M. *et al.* The planar polarity protein Scribble1 is essential for neuronal plasticity and brain function. *J. Neurosci.* **30**, 9738–9752 (2010).
56. Bourin, M. & Hascoët, M. The mouse light/dark box test. *Eur. J. Pharmacol.* **463**, 55–65 (2003).
57. Ortega-Alvaro, A. *et al.* Differential pharmacological regulation of sensorimotor gating deficit in CB1 knockout mice and associated neurochemical and histological alterations. *Neuropsychopharmacology* **40**, 2639–2647 (2015).
58. Brotons-Mas, J.R., Montejo, N., O'Mara, S.M. & Sanchez-Vives, M.V. Stability of subicular place fields across multiple light and dark transitions. *Eur. J. Neurosci.* **32**, 648–658 (2010).
59. Bellistri, E., Aguilar, J., Brotons-Mas, J.R., Foffani, G. & de la Prida, L.M. Basic properties of somatosensory-evoked responses in the dorsal hippocampus of the rat. *J. Physiol. (Lond.)* **591**, 2667–2686 (2013).
60. Fox, S.E. & Ranck, J.B. Jr. Electrophysiological characteristics of hippocampal complex-spike cells and theta cells. *Exp. Brain Res.* **41**, 399–410 (1981).
61. Jeffery, K.J., Gilbert, A., Burton, S. & Strudwick, A. Preserved performance in a hippocampal-dependent spatial task despite complete place cell remapping. *Hippocampus* **13**, 175–189 (2003).
62. Markus, E.J., Barnes, C.A., McNaughton, B.L., Gladden, V.L. & Skaggs, W.E. Spatial information content and reliability of hippocampal CA1 neurons: effects of visual input. *Hippocampus* **4**, 410–421 (1994).

doi:10.1038/nn.4544